

This is a brief description of the methods used in the code for atomic structure calculations (for single-valence systems), and has definitions for all the relevant equations. The code is available online: github.com/benroberts999/ampsci; see the “readme” file for compiling/usage instructions. Some basic documentation for the code is also available: benroberts999.github.io/ampsci/. This is not meant as a complete description of the physics, but references are provided to more detailed descriptions.

1	Radial Dirac equation	1
2	Numerical solution to the Dirac equation	1
3	Hartree-Fock (self-consistent field method)	3
4	Finite basis of orbitals	5
5	External fields & matrix elements	6
6	Correlation corrections	9
7	Correlation potential: Feynman method	10
8	All-orders correlation potential	14
9	Structure radiation + renormalisation	15
10	Relativity beyond Dirac-Coulomb (Breit+QED)	16
11	Demonstration for Cs	19
A	Appendix	21

1 Radial Dirac equation

Using atomic units¹, the single-electron Dirac equation is

$$(h_D - \varepsilon) \phi(\mathbf{r}) = 0, \quad (1)$$

where h_D is the Dirac Hamiltonian (see, e.g., Ref. [1]):

$$h_D = c\boldsymbol{\alpha} \cdot \mathbf{p} + c^2(\beta - 1) + \hat{V}, \quad (2)$$

and $\boldsymbol{\alpha} = \gamma^0 \boldsymbol{\gamma}$ and $\beta = \gamma^0$ are Dirac matrices. Note that we have subtracted the electron rest energy, so the total relativistic energy is $E = \varepsilon + c^2$. For bound states, $\phi \rightarrow 0$ as $r \rightarrow \infty$ and ϕ is regular everywhere and thus normalisable. The set of solutions $\{\phi_i\}$ (including the negative energy states) to (1) form a complete orthogonal set/basis. We use the standard normalisation choice, so that $\langle \phi_i | \phi_j \rangle = \delta_{ij}$. Wavefunctions for many-electron atoms are formed from single-particle orbitals; see Appendix A.1, and Refs. [2, 3].

For spherically symmetric potentials \hat{V} , we can express the four-component single-particle orbitals in the form^{2,3}:

$$\phi_{n\kappa m}(\mathbf{r}) = \frac{1}{r} \begin{pmatrix} f_{n\kappa}(r) \Omega_{\kappa m}(\mathbf{n}) \\ i g_{n\kappa}(r) \Omega_{-\kappa, m}(\mathbf{n}) \end{pmatrix}, \quad (3)$$

where n is the principle quantum number, $\kappa = (l - j)(2j + 1)$ is the Dirac quantum number, $m = j_z$ is the projection of $\mathbf{j} = \mathbf{l} + \mathbf{s}$ (total electron angular momentum) onto the quantisation axis, and Ω is a (two-component) spherical spinor,

$$\Omega_{\kappa m} \equiv \sum_{s_z = \pm 1/2} \langle l, m - s_z, 1/2, s_z | j, m \rangle Y_{l, m - s_z}(\mathbf{n}) \chi_{s_z}, \quad (4)$$

with $\langle j_1 m_1 j_2 m_2 | JM \rangle$ a Clebsch-Gordon coefficient, Y_{lm} a spherical harmonic, $\mathbf{n} = \mathbf{r}/r$, and χ_{s_z} is a spin eigenstate ($s_z = \pm 1/2$). The terms in ϕ are orthonormal as:

$$(n\kappa | n'\kappa) \equiv \int (f_{n\kappa} f_{n'\kappa} + g_{n\kappa} g_{n'\kappa}) dr = \delta_{n'n} \quad (5)$$

$$\langle \kappa m | \kappa' m' \rangle \equiv \int (\Omega_{\kappa m}^\dagger \Omega_{\kappa' m'}) d\Omega = \delta_{\kappa' \kappa} \delta_{m' m}. \quad (6)$$

Then, we can define the radial Dirac equation in the form:

$$(h_r - \varepsilon) F_{n\kappa} = 0, \quad (7)$$

where we defined the *radial spinor*,⁴

$$F_{n\kappa} = \begin{pmatrix} f_{n\kappa}(r) \\ g_{n\kappa}(r) \end{pmatrix}, \quad (8)$$

and *radial Hamiltonian*,

$$h_r = \begin{pmatrix} \hat{V} & c(\frac{\kappa}{r} - \partial_r) \\ c(\frac{\kappa}{r} + \partial_r) & \hat{V} - 2c^2 \end{pmatrix}. \quad (9)$$

The 3D (spherical) Hamiltonian can also be expressed in this form by replacing κ in (9) with $-\hat{k}$ (top right) and \hat{k} (bottom left), where $\hat{k} \equiv -1 - \boldsymbol{\sigma} \cdot \mathbf{l}$, and $\hat{k} \Omega_{\kappa m} = \kappa \Omega_{\kappa m}$. I will suppress the r subscript and use $(h - \varepsilon) F = 0$ and $(h - \varepsilon) \phi = 0$ interchangeably, since there is no risk of confusion.

1.1 Nuclear and electron potentials⁵

For a many-electron atom, the potential term consists of the sum of the nuclear and inter-electron potentials:

$$\hat{V} = V_{\text{nuc}} + V_{\text{el}}. \quad (10)$$

The electron potential involves a large number of complicated terms and must be taken into account approximately (as discussed in the following sections). For a point-like nucleus, $V_{\text{nuc}} = -Z/r$; in reality, the nuclear charge is distributed across the finite-size nucleus. To form V_{nuc} , we assume the nuclear charge is distributed according to a Fermi distribution,

$$\rho(r) = \rho_0 (1 + \exp[(r - c)/a])^{-1}, \quad (11)$$

where ρ_0 is the normalisation factor, ($\int \rho dV = Z$), c is the half-density radius, and a is defined via the 90–10% density fall-off $t \equiv 4a \ln 3$ (known as the “skin thickness”), which we take to be $t = 2.3$ fm for all heavy isotopes. The half-density radius is related to a and r_{rms} , the root-mean-square charge radius, as $c = \sqrt{(5r_{\text{rms}}^2 - 7\pi^2 a^2)}/3$. Then, V_{nuc} is obtained numerically from (11) using Gauss’ law. The code also allows you to assume a spherical nucleus (mainly used for testing).

2 Numerical solution to the Dirac equation⁶

2.1 Bound-state solution to local Dirac equation

From Eqs. (7) and (9), we can express the radial derivative as:

$$\frac{\partial F}{\partial r} = \frac{1}{c} \begin{pmatrix} -c\kappa/r & (\varepsilon - \hat{V} + 2c^2) \\ -(\varepsilon - \hat{V}) & c\kappa/r \end{pmatrix} F, \quad (12)$$

which has the familiar form of an ODE. Very roughly, we can solve an ODE numerically by stepping forward if we know the derivative of a function and the value of the function at some previous point: $F(r + \delta r) \approx F(r) + \partial_r F \delta r$. Multi-step methods approximate the value of the derivative along the interval $(r, r + \delta r)$ with greater accuracy by using several points in the

¹ $\hbar = m_e = e = |e| = 1$, $c = 1/\alpha \approx 137$ ($e > 0$, electron has charge $-e$).

²We use the Dirac representation; see Appendix A.6.

³Our notation differs from some other places: compared to Ref. [1] we have $f \leftrightarrow g$; compared to [3] we have $f_{\text{here}} = P_{\text{Johnson}}$, $g_{\text{here}} = -Q_{\text{Johnson}}$; compared to Ref. [4] we have $g_{\text{here}} = \alpha g_{\text{Dzubia}}$; and compared to Ref. [5] we have $f_{\text{here}} = g_{\text{Sapirstein}}$ and $g_{\text{here}} = -f_{\text{Sapirstein}}$.

⁴Radial spinor defined in: `/src/Wavefunction/DiracSpinor.hpp`

⁵Nuclear potentials defined in: `/src/Physics/NuclearPotentials.hpp`

⁶Functions to solve Dirac equation defined in: `/src/DiracODE/`

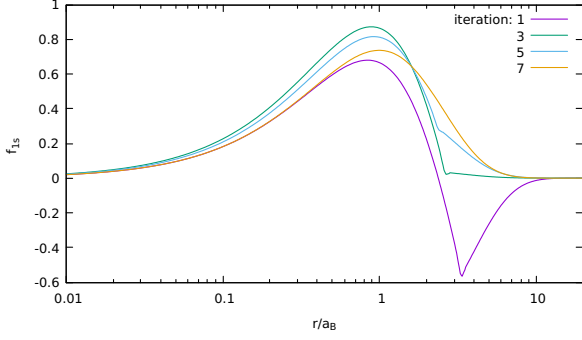


Figure 1: Hydrogen $1s$ orbital $[f(r)]$, as calculated at the first though 7th iteration. For this example, the initial energy guess was $-0.3a_u$, and converged to $-0.500006566..$ to parts in 10^{-16} in 12 iterations.

estimation. We use an M -step Adams-Moulton method, which, for a general DE of the form $\partial_r F_n = y_n$, has the form

$$F_{n+M} = F_{n+M-1} + \delta r \sum_{i=0}^M b_i y_{n+i}, \quad (13)$$

where $y_n \equiv y(r_n)$, and b_j are numerical coefficients. Since the derivative Eq. (12) can be written as a matrix equation, we can solve this equation for F_{n+M} algebraically:

$$F_{n+M} = [1 - \delta r b_M D_{n+M}]^{-1} \left(F_{n+M-1} + \delta r \sum_{i=0}^{M-1} b_i D_{n+i} F_{n+i} \right). \quad (14)$$

Therefore, we may find the value of the function at $n + M$ grid-point, provided $M - 1$ previous points are known. These initial points are determined by solving the asymptotic form of the Dirac equation analytically accounting for the boundary conditions (see Ref. [3] for details), noting that for neutral atoms $V(r) \approx -Z/r$ for small r , and $\approx -1/r$ for large r .

Equation (12) has solutions for any given ε . We are interested in the specific bound-state solutions [$F \rightarrow 0$ as $r \rightarrow \infty$, and $F(0) = 0$], which occur for specific values of ε . To solve the bound-state (eigenvalue) problem, an initial ε is guessed, and the DE is solved using the multi-step method. Then, small adjustments are made to ε until (a) we have the correct state ($n\kappa$) determined by the number of nodes of the orbital ($n - l - 1$) [1], and (b) we have the correct boundary conditions.

It is common to expand the orbital around $r = 0$ to start the procedure, and then adjust the energy until $F \rightarrow 0$ at infinity. A more numerically stable approach is to solve the DE twice, once starting from $r = 0$, and once from $r = \infty$ [3]. These two solutions are stepped inwards toward some central point, where the two solutions are joined – one of the two solutions is re-scaled so that $f_0 = f_\infty$ at the defined point. Small energy adjustments are made until the lower g components also match at this point (this ensures the derivatives match, and the join is smooth). In our case, the two solutions are not joined at a single point, but are instead “meshed” across a few (~ 10) points around the classical turning point, defined via $V(r_{\text{ctp}}) = \varepsilon$. The meshing procedure acts to suppress numerical noise, and makes the method more stable. This procedure typically allows convergence of the energies to parts in 10^{16} ; see, e.g., Fig. 1.

Note that Eq. (12) does not determine the normalisation for F , so the solutions must be normalised explicitly [Eq. (5)]. Further, the sign of F is also arbitrary from Eq. (12); we choose $f(r)$ to be positive as $r \rightarrow 0$, as is standard.

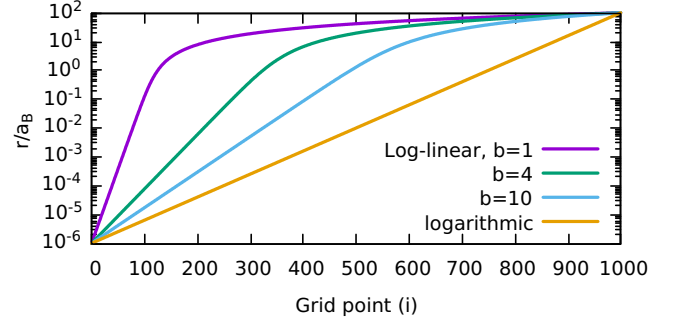


Figure 2: Radial distance r_i as function of grid-point, i .

Everywhere in the code, the fine structure constant is replaced with: $\alpha \rightarrow \lambda \alpha_0$ (in atomic units, $\alpha = 1/c$), where $\alpha_0 \approx 1/137$. The factor λ is a run-time input option, that is 1 by default. For example, letting $\lambda \rightarrow 0$ (i.e., $c \rightarrow \infty$) allows us to perform calculations in the non-relativistic limit. This is a particularly useful option for checking the calculations, and for determining the sensitivity of particular observables to variations in the fine structure constant. Modifications can also be made to the above equations to account for the finite electron/nucleus mass (reduced mass) – but this is not implemented in the code.

2.2 Radial grid⁷

The equations are solved numerically on a finite radial grid (the orbitals are stored in arrays on this grid). We define a grid on the region from r_0 to r_{max} , that has N points.

We don’t use a uniformly spaced grid, since the wavefunctions vary very rapidly at small distances, but rather slowly at large distances. We define a non-uniformly-spaced radial grid (r_i) in terms of a uniformly spaced u grid ($u_{i+1} = u_i + \delta u$). In this case, integrals become:

$$\int_0^\infty f(r) dr \rightarrow \int_{r_0}^{r_{\text{max}}} f(r) dr \rightarrow \int_{u_0}^{u_{\text{max}}} f(r(u)) \frac{dr}{du} du, \quad (15)$$

which numerically becomes:

$$\int_{u_0}^{u_{\text{max}}} f(r(u)) \frac{dr}{du} du \rightarrow \sum_{i=0}^{N-1} f(r_i) \frac{dr}{du} \Big|_i \delta u \quad (16)$$

(in the code we actually use a quadrature integration formula for the integrals). The initial/final grid points and the grid spacings must be chosen such that the above numerical approximations are sufficiently accurate.

In the code, we can set either a logarithmic grid, defined:

$$u = \ln(r), \quad \frac{dr}{du} = r, \quad (17)$$

or a mixed log-linear grid, defined:

$$u = r + b \ln(r), \quad \frac{dr}{du} = \frac{r}{r+b}, \quad (18)$$

which is approximately logarithmic at small distances ($r < b$), and approximately linear at large distances (typically $b \sim 10 a_0$); see Fig. 2. The logarithmic grid works very well, and allows good convergence without requiring a large number of points, but works less well for highly excited states, and works quite poorly for continuum states with high energy. The log-linear grid works well in a wide range of cases, but often needs more grid points to achieve the same numerical accuracy.

⁷Radial grid defined in: `/src/Maths/Grid.hpp`

2.3 Dirac equation involving inhomogeneous or non-local terms (Green's Method)⁸

This is a brief overview; for details see, e.g., Ref. [6]. Consider the inhomogeneous Dirac equation, with ‘source’ term S :

$$(h_l - \varepsilon) F = S, \quad (19)$$

where h_l is a Dirac Hamiltonian involving only local potential terms. We solve this for a normalisable F using the Green's method for ODEs. First, take the homogeneous equation:

$$(h_l - \varepsilon) G = 0, \quad (20)$$

which we solve (for a given energy ε) using the regular linear ODE multi-step methods from Sec. 2.1. Note that since F is a normalisable solution to (19) G will *not* (in general) be a normalisable solution to (20) [i.e., G is not regular at the origin/infinity]. Instead, we seek two solutions, which are each bound by one of the boundary conditions; i.e., one solution that satisfies the boundary condition at the origin, G_0 , and a second that satisfies that at infinity, G_∞ . Then, the normalisable solution to (19) that satisfies both boundary conditions is:

$$F(r) = G_\infty(r) \int_0^r \frac{G_0(r')^T S(r')}{c w(r')} dr' r' + G_0(r) \int_r^\infty \frac{G_\infty(r')^T S(r')}{c w(r')} dr' \quad (21)$$

($A^T B \equiv f_A f_B + g_A g_B$) where $c = 1/\alpha$. The Wronskian,

$$w(r) = f_\infty(r) g_0(r) - f_0(r) g_\infty(r), \quad (22)$$

should be independent of r .

Note that this method clearly doesn't work if $w = 0$; worse, the method can be numerically unstable if S and w are both small (if S is too small, it implies the $G_{0,\infty}$ solutions will be similar, and thus w will be small).

2.4 Continuum orbitals

We are sometimes interested in continuum orbitals that are regular at the origin (see, e.g., Ref. [1]). For continuum orbitals of the desired energy $\varepsilon > 0$, we solve using the multi-step method described above, starting from the origin and integrating outwards. Note that we do not have $F_c \rightarrow 0$ at large r , and continuum orbitals cannot be normalised as above. For most problems, however, we do require normalised orbitals.

We choose energy normalisation [1]:

$$\int_{\varepsilon-\delta\varepsilon}^{\varepsilon+\delta\varepsilon} \langle \varepsilon' \kappa m | \varepsilon \kappa m \rangle d\varepsilon' = 1. \quad (23)$$

This equation cannot be used directly. Instead, the orbitals are normalised in analogy with analytic Coulomb (H-like) continuum states. For Coulomb potentials, at large r we have:

$$f(r) \approx \sqrt{\frac{\alpha}{\pi\beta}} \sin(kr + \dots), \quad (24)$$

with $\beta = \sqrt{\varepsilon/(\varepsilon + 2c^2)}$ (other terms in sine function are either constant, or logarithmic in r). At large r , the atomic potential is also Coulomb-like. We use (24) to normalise the orbitals by

enforcing the amplitude of the sine-like orbitals at large r to match the analytic H-like solutions [1].

To do this, we have to extend the radial grid out to very large distances, often much larger than the normal grid used to solve the bound-state orbitals. The orbital is solved out to large r until the amplitude/frequency of the oscillations becomes close enough to constant, and then the amplitude is re-scaled to match (24). After solving, the orbital is only kept up until r_{\max} , since larger distances typically do not contribute to any required radial integrals.

3 Hartree-Fock (self-consistent field method)⁹

The many-body atomic Hamiltonian may be expressed as

$$H = \sum_i \hat{h}_0(\mathbf{r}_i) + \sum_{i < j} \frac{1}{|\mathbf{r}_i - \mathbf{r}_j|}, \quad (25)$$

where

$$\hat{h}_0 = c\boldsymbol{\alpha} \cdot \mathbf{p} + c^2(\beta - 1) + V_{\text{nuc}},$$

is the single-particle Dirac Hamiltonian including only the nuclear potential (see Sec. A.1). To solve the Dirac equation for an N electron atom, we replace the complicated electron-electron repulsion term with an approximate potential, $V_{\text{avg}}^{(i)}$, which is the average potential seen by the i th electron due to the other $(N - 1)$ electrons:

$$H \approx \sum_i \left[\hat{h}_0(\mathbf{r}_i) + \hat{V}_{\text{avg}}^{(i)}(\mathbf{r}_i) \right]. \quad (26)$$

For any general ‘self-consistent field method’, we start with an initial approximation for the electronic potential (e.g., Thomas-Fermi potential, or a simple parametric potential), and use this to generate a set of orbitals for the desired subset of atomic electrons (e.g., the core). The total electron density formed from these orbital tells us the electronic charge distribution across the atom, which we use to generate a new electronic potential (Gauss' law). In general, this new potential will be a better approximation for the true electronic potential than the initial guess. A new set of orbitals formed in this better potential will be a better set of orbitals, which we use to generate a better-yet potential and so on, until convergence is reached. At the end, the potential used to form the electron orbitals should be the same as the potential that is formed from the electron orbitals, and is thus self-consistent.

3.1 Relativistic Hartree-Fock method

The self-consistent method we use is the relativistic Hartree-Fock (HF) method, which includes the electron exchange interaction. This section largely follows the detailed explanation from Ref. [3], with a few extensions. In this approximation, the single-particle Dirac equation is

$$(h_{\text{HF}} - \varepsilon) \phi(\mathbf{r}) = 0, \quad (27)$$

with the Hartree-Fock Hamiltonian,

$$h_{\text{HF}} = c\boldsymbol{\alpha} \cdot \mathbf{p} + c^2(\beta - 1) + V_{\text{nuc}} + \hat{V}_{\text{HF}}. \quad (28)$$

Here, \hat{V}_{HF} is the Hartree-Fock potential. We consider mainly atoms with a single valence electron above closed shells, and

⁸Implemented: /src/DiracODE/Adams.Greens.hpp

⁹Implemented in: /src/HF/HartreeFock.hpp

take the Hartree-Fock potential to be the potential due to the $N - 1$ core electrons. This is called the $V^{(N-1)}$ potential.

By minimising the many-body energy for the single Slater-determinant electronic wavefunction (see, e.g., Ref. [3]), the Hartree-Fock potential can be derived as

$$\hat{V}_{\text{HF}}\phi_a(\mathbf{r}_1) = \sum_{i \neq a}^{N_c} \left(\int \frac{\phi_i^\dagger(\mathbf{r}_2)\phi_i(\mathbf{r}_2)}{|\mathbf{r}_{12}|} d^3\mathbf{r}_2 \phi_a(\mathbf{r}_1) - \int \frac{\phi_i^\dagger(\mathbf{r}_2)\phi_a(\mathbf{r}_2)}{|\mathbf{r}_{12}|} d^3\mathbf{r}_2 \phi_i(\mathbf{r}_1) \right), \quad (29)$$

where the sum over i extends over all occupied electrons $i = \{n_i, \kappa_i, m_i\}$. The first and second terms are the direct and exchange parts, respectively (the ‘Hartree’ method neglects the exchange part). The Coulomb integrals are computed by expanding r_{12}^{-1} in terms of spherical harmonics (Laplace expansion) – see Appendix A.4. Integrating over angles, and summing over m quantum numbers we have:

$$\hat{V}_{\text{HF}}F_a(r) = \left(\sum_b [j_b] x_b y_{bb}^0(r) \right) F_a(r) - \frac{1}{[j_a]} \sum_b \tilde{x}_b^a \sum_k (C_{ab}^k)^2 y_{ab}^k(r) F_b(r) \quad (30)$$

$$\equiv V_{\text{dir}}(r) F_a(r) + [\hat{V}_{\text{ex}}F_a](r), \quad (31)$$

where now the b sum extends over all occupied *orbitals* (i.e., $b = \{n_b, \kappa_b\}$), y_{ab}^k is a *Hartree screening function* (see A.4):

$$y_{ab}^k(r) = \int_0^\infty \frac{r_{<}^k}{r_{>}^{k+1}} [f_a f_b + g_a g_b](r') dr', \quad (32)$$

with $r_{<} = \min(r, r')$, and C_{ab}^k is the angular factor (A.4),

$$C_{ab}^k \equiv \langle \kappa_a || C^k || \kappa_b \rangle = (-1)^{j_a+1/2} \sqrt{[j_a][j_b]} \times \begin{pmatrix} j_a & j_b & k \\ -1/2 & 1/2 & 0 \end{pmatrix} \pi(l_a + l_b + k). \quad (33)$$

Here, $\pi(l) = 1(0)$ if l is even(odd) (parity selection rule), and $[j] \equiv 2j + 1$. The x_b is the occupation fraction for core shell b (typically $x_b = 1$), and $\tilde{x}_b^a = x_b$ for $b \neq a$, $\tilde{x}_a^a = 1$; this is an approximate treatment for open-shell systems¹⁰.

First, the Hartree-Fock equations (27), (29) are solved self-consistently for all the electrons in the core. Since the HF potential depends on the electron orbitals (which depend on the HF potential), this equation must be solved iteratively, starting from an initial approximation for the potential. Once the self-consistency is reached, the core orbitals are ‘frozen’. Then we do the same procedure for the valence electrons; the exchange part of the HF potential depends on the valence orbital, so these equations must also be solved iteratively. Plots of the electron density ($\rho = \sum_n |\psi_n|^2$) for Cs are shown in Fig. 3, as calculated in varying approximations.

The Hartree-Fock method is the ideal starting point for many-body calculations, since all first-order corrections to the HF potential (i.e., corrections involving single electron excitations) cancel exactly [2]. Corrections to energies and wavefunctions only arise at the second-order of perturbation theory.

¹⁰The i sum in (29) includes a sum over all occupied m states; for partially filled shells, this doesn’t include all m values. So, to do the sum, we assume each m is filled with equal probability – i.e., that each m is partially filled. We assume non-relativistic filling (e.g., $p_{1/2}$ and $p_{3/2}$ on equal footing).

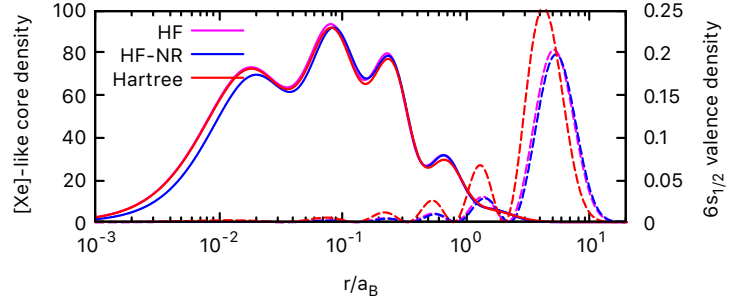


Figure 3: Electron density $\rho = \sum_n |\psi_n|^2$ for the core (solid line) and $6s_{1/2}$ valence (dashed line) electrons for Cs in the relativistic Hartree-Fock (HF), non-relativistic Hartree-Fock (HF-NR), and Hartree approximations. Relativistic effects ‘pull’ the electrons closer to the nucleus, and the exchange interaction is crucial for valence states.

3.2 Solving the HF equation for given orbital

To solve the HF equation for a given orbital, we use the Green’s method as outlined above. The HF Hamiltonian is split in to local and non-local parts as $h_{\text{HF}} = h_l + V_{\text{nl}}$, with

$$h_l = h_0 + V_{\text{nuc}} + fV_{\text{dir}}, \quad (34)$$

$$V_{\text{nl}} = (1 - f)V_{\text{dir}} + V_{\text{exch}}. \quad (35)$$

Here,

$$f = \begin{cases} (N_c - 1)/N_c & \text{core} \\ 1 & \text{valence} \end{cases} \quad (36)$$

is chosen so that $V_l = V_{\text{nuc}} + fV_{\text{dir}} \rightarrow -Z_{\text{ion}}/r$ as $r \rightarrow \infty$ (otherwise, we would have $V_l \rightarrow 0$). This is done to ensure the existence of the solution that is regular at infinity (G_∞), and so that the asymptotic behaviour of the homogeneous solutions (20) match that of the final solution.

Then, the inhomogeneous equation has the form of Eq. (19):

$$(h_l - \varepsilon) F = -V_{\text{nl}} F. \quad (37)$$

Note that the ‘source’ term in this case contains the solution F . So the equations must be solved iteratively, with some starting approximation for the source term, so that the solution at the n th step depends on the approximate solution from the previous step. Further, V_{nl} and h_l also depend on the solution F via (31), and these are also formed at the n th step using $F^{(n-1)}$. That is, the equation we solve at each iteration is

$$\left(h_0 + V_{\text{nuc}} + fV_{\text{dir}}^{(n-1)} - \varepsilon \right) F^{(n)} = - \left((1 - f)V_{\text{dir}}^{(n-1)} + V_{\text{exch}}^{(n-1)} \right) F^{(n-1)}. \quad (38)$$

The energy guess used for the $(n+1)$ th step can be approximated from $\Delta V^{(n)} \equiv V_{\text{HF}}^{(n)} - V_{\text{HF}}^{(n-1)}$, as $\varepsilon^{(n)} + \delta\varepsilon$:

$$\delta\varepsilon \approx \frac{\langle F^{(n-1)} | \Delta V | F^{(n)} \rangle}{\langle F^{(n-1)} | F^{(n)} \rangle}. \quad (39)$$

In general, these solutions will not be correctly normalised eigenstates of the HF Hamiltonian. We therefore make small adjustments to the energy and orbital until F is properly normalised and thus an eigenstate of the Hamiltonian. This procedure is outlined in the next subsection 3.3.

Once the energy has been fine-tuned, and we have a normalised eigenstate, we continue the HF procedure. To aid convergence, however, we first “damp” the orbitals as:

$$F \rightarrow (1 - \eta)F + \eta F_{\text{old}}. \quad (40)$$

This both increases the numerical stability, and speeds up the convergence. So long as the equations converge, the solutions do not depend on the value chosen.

3.3 Energy adjustments – finding eigenstate

Assume the correct orbital and energy can be written as $F + \delta F$, and $\varepsilon + \delta\varepsilon$, where F was the solution to Eq. (38) using the trial energy ε . Subbing this back into the HF equation, we find a new inhomogenous equation (to first order):

$$(h_{\text{HF}} - \varepsilon)\delta F = \delta\varepsilon F \quad (41)$$

$$(h_1 - \varepsilon)\delta F = \delta\varepsilon F - V_{\text{nl}}\delta F, \quad (42)$$

which we solve iteratively for δF and $\delta\varepsilon$. As the first step, we divide (42) by the unknown $\delta\varepsilon$, set $V_{\text{nl}}\delta F = 0$, and solve for $\tilde{F} \equiv \delta F/\delta\varepsilon$ using Green’s method (21). Note that we don’t need to re-solve the homogeneous equation (20), since we can re-use the G_∞ , G_0 solutions obtained when solving (38).

Since $(F + \delta F)$ must be normalised, we find the first guess for $\delta\varepsilon$ as (keeping only first-order terms):

$$\delta\varepsilon = \frac{\langle F|\tilde{F}\rangle - 1}{2\langle F|\tilde{F}\rangle}. \quad (43)$$

Using $\delta F = \delta\varepsilon\tilde{F}$, we form $V_{\text{nl}}\delta F$ and solve (42) for δF . Then, we make the corrections to the orbital and energy:

$$F \rightarrow F + \delta F, \quad \varepsilon \rightarrow \varepsilon + \delta\varepsilon. \quad (44)$$

This iterative procedure is continued from Eq. (42) until the energy correction drops below a specified value (i.e., until F is properly normalised). This procedure is very rapid; e.g., $\delta\varepsilon/\varepsilon$ typically converges to parts in 10^{20} with just two iterations.

Note that, so long as it was chosen appropriately, the non-local term V_{nl} is small, and so the $V_{\text{nl}}\delta F$ term is even smaller and can be excluded entirely in this section without having much of an impact. Including it, however, leads to better overall convergence of the HF equations. Note that $V_{\text{nl}}\delta F$ includes $V_{\text{exch}}\delta F$, which must be calculated.

3.4 Approximate “local” exchange potential

There are several methods for obtaining a localised approximation to the HF potential, common examples are the “Hartree-Fock-Slater” [7], and Kohn-Sham methods. Here, I outline a different method that very well approximates the HF potential. We use this only as a starting point for the HF (and TDHF) procedure, so final result do not depend on this potential. A good choice of starting approximation does, however, speed up the convergence of the iterative procedures.

Introducing the notation v_{ab}^x [see Eq. (30)], the non-local exchange part of the HF potential can be expressed

$$[\hat{V}_{\text{ex}}F_a](r) = \sum_b v_{ab}^x(r)F_b(r). \quad (45)$$

Multiply (45) from the right and divide by $F_a^\dagger F_a$:

$$\frac{[\hat{V}_{\text{ex}}F_a]F_a^\dagger}{F_a^\dagger F_a}F_a = \frac{\sum_b v_{ab}^x(r)F_b(r)F_a^\dagger(r)}{F_a^\dagger F_a}F_a(r) \quad (46)$$

$$\approx U_{\text{ex}}^{(a)}(r)F_a(r). \quad (47)$$

In this way we may define $U_{\text{ex}}^{(a)}(r)$, which is a localised exchange potential (for state a). Note that $U(r)$ is different for each state, and depends on F_a , and therefore must be found iteratively.

This is numerically unstable when $F_a^\dagger F_a$ is small. However, when F_a is small, the exchange potential is less important (only the combination $V_{\text{ex}}F_a$ enters the equations). We proceed by introducing a cut-off, λ_a , so that

$$U_{\text{ex}}^{(a)}(r) = v_{aa}^x(r) + \sum_{b \neq a} v_{ab}^x(r)\Lambda(r), \quad (48)$$

$$\Lambda(r) = \begin{cases} \frac{F_a^\dagger(r)F_b(r)}{F_a^\dagger F_a} & |f_a(r)| > \lambda_a \\ 0 & \text{otherwise} \end{cases}. \quad (49)$$

We don’t apply the cut-off for the $b = a$ term, since there is exact cancellation and no numerical instability. This $a = b$ term gives the dominant contribution to the exchange potential. The reason this method gives such good results is that the dominating case is treated exactly. In the code, the cut-off is taken as $\lambda_a = 10^{-2}|f_a|^{\text{max}}$, where $|f|^{\text{max}}$ is the maximum magnitude for the upper $f(r)$ component of F_a . Making the cut-off too small introduces numerical instabilities.

4 Finite basis of orbitals¹¹

In many problems in perturbation theory, a summation over the full (infinite) set of orbitals is required. In theory, a basis of HF orbitals can be used for this. However, such a basis generally converges very slowly, requires a very large radial grid, and the solutions become numerically unstable for low energies. Further, sum over all states must include the integral over all positive- and negative-energy continuum states. Instead, it is common to introduce a finite basis for the radial Dirac equation, see, e.g., Ref. [8, 9]. We assert that all orbitals go to zero at the boundary of a subset of the radial grid, r_{max} . This is equivalent to placing the atom in the centre of an infinite spherical “square-well” potential. In this case, a complete set of orbitals can be approximately expanded in terms of a finite number of discrete states. So long as the size of the cavity is large compared to typical radius of orbitals we are directly interested in, the results should be independent of the cavity size.

4.1 B-spline basis (algebraic solution to Dirac eq.)

The set of atomic orbitals are expanded as

$$F_{n\kappa} = \sum_i^{2N} p_i S_i(r), \quad (50)$$

where $\{S_i\}$ are a set of $2N$ basis orbitals that form a complete set over a sub-domain of the radial grid $[0, r_{\text{max}}]$ (N is defined this way because of the dual set of positive/negative energy Dirac solutions). The $\{p_i\}$ expansion coefficients are found by diagonalising the set of basis orbitals with respect to the Hamiltonian matrix, equivalent to solving the eigenvalue problem:

$$\langle S_i|\hat{h}_{\text{HF}}|S_j\rangle p_i = \varepsilon \langle S_i|S_j\rangle p_i. \quad (51)$$

There are $2N$ solutions of eigenvalues ε with corresponding eigenvectors \vec{p} , which correspond to the spectrum of stationary states; N of these correspond to negative-energy ($\varepsilon < -mc^2$) states. If the $\{S\}$ set is orthonormal, S_{ij} is just the identity;

¹¹Implemented in: /src/Wavefunction/BSplineBasis.hpp

Table 1: Comparison between energies of spline (DKB) basis orbitals and finite-difference Hartree-Fock orbitals. The basis was constructed using 50 B-splines of order 7 in a cavity of radius $30 a_B$ with the first internal point at $r = 10^{-5} a_B$ (only the first 10 splines of each symmetry are shown). Final column shows the root-mean-square radii for the Hartree-Fock orbitals. The spline basis energies agree very well (better than parts in 10^6) with the Hartree-Fock energies, so long as the cavity is large compared to the typical radius of the orbital in question; for higher orbitals, where this is not the case, the energies diverge significantly. [$\epsilon = (A - B)/A$]

n	$s_{1/2}$				$p_{1/2}$			
	ϵ_{spline}	ϵ_{HF}	ϵ	$\langle r^2 \rangle_{\text{HF}}^{1/2}$	ϵ_{spline}	ϵ_{HF}	ϵ	$\langle r^2 \rangle_{\text{HF}}^{1/2}$
1	-1330.1186542	-1330.1188558	$-2e-7$	0.03				
2	-212.5644469	-212.5644963	$-2e-7$	0.12	-199.4294948	-199.4295038	$-5e-8$	0.10
3	-45.9697097	-45.9697486	$-8e-7$	0.32	-40.4482937	-40.4483086	$-4e-7$	0.31
4	-9.5127994	-9.5128206	$-2e-6$	0.74	-7.4462753	-7.4462846	$-1e-6$	0.77
5	-1.4898011	-1.4898044	$-2e-6$	1.88	-0.9078963	-0.9078975	$-1e-6$	2.15
6	-0.1273679	-0.1273681	$-1e-6$	6.52	-0.0856153	-0.0856159	$-6e-6$	8.65
7	-0.055047	-0.0551874	$-3e-3$	14.58	-0.0411125	-0.0420214	$-2e-2$	18.16
8	-0.0240059	-0.0309525	$-3e-1$	25.77	-0.0110954	-0.0251205	$-8e-1$	30.79
9	0.0147887	-0.0198146		40.11	0.0314743	-0.0167280		46.56
10	0.0679063	-0.0137713		57.61	0.0877553	-0.0119427		65.48

Table 2: Magnetic dipole hyperfine constants A (MHz) for single-particle s -state Cs orbitals (point-like nuclear magnetisation distribution). Calculated using the Hartree-Fock orbitals, and the DKB basis constructed using 50 B-splines of order 7 in a cavity of radius $50 a_B$, with varying first internal point (A is sensitive to orbitals at small radial distances). [$\epsilon = (A - B)/A$]

n	A_{HF}	$r_0 = 10^{-4} a_B$		$10^{-5} a_B$		$10^{-6} a_B$	
		$A_{\text{spline}}, \epsilon$		$A_{\text{spline}}, \epsilon$		$A_{\text{spline}}, \epsilon$	
1	3.9180×10^7	3.8361×10^7	-2×10^{-2}	3.9172×10^7	-2×10^{-4}	3.9179×10^7	-3×10^{-6}
2	4.6208×10^6	4.5209×10^6	-2×10^{-2}	4.6199×10^6	-2×10^{-4}	4.6207×10^6	-3×10^{-6}
3	9.3463×10^5	9.1437×10^5	-2×10^{-2}	9.3446×10^5	-2×10^{-4}	9.3462×10^5	-1×10^{-5}
4	1.9822×10^5	1.9392×10^5	-2×10^{-2}	1.9819×10^5	-2×10^{-4}	1.9823×10^5	4×10^{-5}
5	2.7987×10^4	2.7380×10^4	-2×10^{-2}	2.7982×10^4	-2×10^{-4}	2.7988×10^4	5×10^{-5}
6	1.4337×10^3	1.4022×10^3	-2×10^{-2}	1.4334×10^3	-2×10^{-4}	1.4336×10^3	-4×10^{-5}

in general it is not. Both h_{ij} and S_{ij} are positive-definite real matrices. States of different κ are orthogonal, so the h_{ij} matrix can be chosen to be block diagonal (in κ); i.e. the expansion may be performed separately for each κ .

The choice of basis must account for the boundary conditions for the stationary states. A good choice of basis allows for convergence of many-body problems with fewer basis states. The particular choice we use is called the Dual-Kinetic-Balance (DKB) B-spline basis as introduced in Ref. [10];

$$S_i^{\text{DKB}} = \begin{cases} \begin{pmatrix} b_i(r) \\ \frac{\alpha}{2} (\partial_r + \kappa/r) b_i(r) \end{pmatrix} & 0 \leq i < N \\ \begin{pmatrix} \frac{\alpha}{2} (\partial_r - \kappa/r) b_{i-N}(r) \\ b_{i-N}(r) \end{pmatrix} & N \leq i < 2N. \end{cases} \quad (52)$$

full details, including on including boundary conditions, are given in that work (see also [9, 11]). Note that the boundary conditions are met by discarding some of the underlying $b_i(r)$ b-splines; when we talk of an expansion using N splines, we refer only to the ones that are kept; the underlying spline basis consists of a slightly larger set [10]. Another common choice, which we refer to as the Notre-Dame (ND) basis [9] may be formed with the lower-component of (52) set to zero for $i < N$, and the upper set to zero for $i \geq N$; this set requires extra conditions for the boundary conditions to be met [9].

Each B-spline, $b_i^{(k)}(r)$, is a polynomial of degree $k-1$, that is non-zero only in the interval $t_i \leq r < t_{i+k}$, where $\{t_i\}$ are a set of $(N+k-2)$ “knots” (the S_i basis orbitals are non-zero also only in this region). The first “interior” knot is placed at r_0 and the last at r_{max} ¹², and the rest are distributed uniformly along the

u radial grid (see Sec. 2.2). The piecewise nature of the splines simplifies the integrals, and makes H_{ij} and S_{ij} banded matrices, which can typically be solved with high numerical precision.

The basis orbitals are typically defined on a smaller sub-domain of the radial grid. The benefit of restricting the radial sub-domain for the basis is that reasonable completeness can be achieved with fewer basis functions. However, increasing r_0 too much loses the low- r behaviour of the basis orbitals, and making r_{max} too small loses the correspondence between the “real” and basis orbitals. The ideal choice of sub-domain depends on the specifics of the problem. Table 1 shows the energies of spline orbitals, using 50 B-splines of order 7 in a cavity of radius $30 a_B$ with the first internal point at $r = 10^{-5} a_B$. This spline basis is orthogonal (or normal) with respect to the Hartree-Fock core to parts in 10^6 ; the basis itself is orthogonal to parts in 10^{15} . Table 2 shows hyperfine constants calculated using spline orbitals, which is a test of the low- r performance of the orbitals.¹³

5 External fields & matrix elements¹⁴

5.1 Time-dependent Hartree-Fock

In the presence of a time-varying external field of frequency ω ,

$$\hat{F} = \hat{h}e^{-i\omega t} + \hat{h}^\dagger e^{i\omega t}, \quad (53)$$

where \hat{h} is a tensor operator of rank k , the orbitals will contain time-varying perturbations:

$$\psi \rightarrow \psi + \delta\psi(t) = \psi + X e^{-i\omega t} + Y e^{i\omega t}, \quad (54)$$

¹³The input files used to generate these tables are provided in: /doc/examples/Cs.testBasis.in

¹⁴Implemented in: /src/ExternalField/

¹²The actual first knot is placed at 0; the end knots are repeated k times.

and $\varepsilon \rightarrow \varepsilon + \delta\varepsilon(e^{-i\omega t} + e^{i\omega t})$. Keeping terms only to first-order, the corrections are seen to satisfy the equations (e.g., [12]):

$$\begin{aligned} (h_{\text{HF}} - \varepsilon - \omega) X &= -(\hat{h} + \delta V - \delta\varepsilon) \psi \\ (h_{\text{HF}} - \varepsilon + \omega) Y &= -(\hat{h}^\dagger + \delta V^\dagger - \delta\varepsilon) \psi, \end{aligned} \quad (55)$$

and $\delta\varepsilon = \langle \psi | \hat{h} + \delta V | \psi \rangle$. Here, δV is the correction to the HF potential arising due to the corrections $\{X^{(c)}, Y^{(c)}\}$ to each of the core orbitals, c ; this will be discussed below. In general, the equations (55) are called the “mixed-states” equations; when they are included into the Hartree-Fock equations, it is known as the time-dependent Hartree-Fock (TDHF) method.

Note that $\delta\psi$ is not (in general) a state of definite angular momentum (hence ‘mixed-states’). This is because the tensor operator \hat{h} may not conserve (electron) angular momentum. We expand X and Y in terms of states χ and η of definite κ (j^π):

$$\begin{aligned} X^{a,m_a} &= \sum_{\alpha,m_\alpha} X_{\alpha,m_\alpha} \\ &= \sum_{\alpha,m_\alpha} (-1)^{j_\alpha-m_\alpha} \begin{pmatrix} j_\alpha & k & j_a \\ -m_\alpha & q & m_a \end{pmatrix} \chi_{\alpha,m_\alpha}. \end{aligned} \quad (56)$$

The superscript refers to the unperturbed state that X is a correction to (here $a \equiv n_a, \kappa_a$). The sum over α runs over all angular momentum states with $j_\alpha = j_a - k, \dots, j_a + k$ and parity $\pi_\alpha = (-1)^{l_a+\pi}$ (π is the parity of the operator \hat{h}). Note that $\{\chi_\alpha\}$ are orthogonal (and are orthogonal to ψ), and form a linearly independent set of solutions to (55).

The corrections may be expressed to lowest-order as:

$$\begin{aligned} |\chi_\alpha\rangle &= \sum_{n \neq a} \frac{|n\rangle \langle n | \hat{h} + \delta V | a \rangle}{\varepsilon_a - \varepsilon_n + \omega} \\ |\eta_\alpha\rangle &= \sum_{n \neq a} \frac{|n\rangle \langle n | \hat{h}^\dagger + \delta V^\dagger | a \rangle}{\varepsilon_a - \varepsilon_n - \omega}, \end{aligned} \quad (57)$$

and it is possible to calculate them that way. Instead, we solve the mixed-states equations (55) without the need for a basis.

5.2 Solving the mixed-states equations¹⁵

The δV term in (55) is very important and will be discussed in the next section. Here, we will ignore how it is calculated and just focus on solving the inhomogeneous equations.

As before, we express the Hamiltonian as $H = H_1 + V_{\text{nl}}$:

$$H_1 = H_0 + V_{\text{nuc}} + V_{\text{dir}} + U_x \quad (58)$$

$$V_{\text{nl}} = V_{\text{exch}} - U_x, \quad (59)$$

where U_x is a local approximation to the exchange potential. In the simplest case it is $(f-1)V_{\text{dir}}$, but better approximations aid the convergence (see Sec. 3.4).

We solve the equations iteratively, such that at the n th step:

$$\begin{aligned} (H_1 - \varepsilon \pm \omega) X^{(n)} &= \\ &= (V_{\text{nl}} X)^{(n-1)} - (\hat{h} + \delta V - \delta\varepsilon^{(n-1)}) \psi_a, \end{aligned} \quad (60)$$

with $V_{\text{nl}} X = 0$ initially. From Eq. (21), the solution is

$$X_\alpha = \frac{X_\alpha^\infty}{cw} \int_0^r \{X_\alpha^0 | S\} r^2 dr' + \frac{X_\alpha^0}{cw} \int_r^\infty \{X_\alpha^\infty | S\} r^2 dr', \quad (61)$$

¹⁵Functions for solving the mixed-states/TDHF equations are in: /src/ExternalField/MixedStates.hpp

Table 3: Testing TDHF method using Eq. (65) for Cs, with $m = 6p_{1/2}$, $\psi = 6s_{1/2}$ (Hartree-Fock level, no δV).

Operator	(65) lhs	(65) rhs	ϵ^*
$h_{\text{E1}} (\omega = \omega_{\text{HF}})$	63.2029312	63.2025676	6×10^{-6}
$h_{\text{E1}} (\omega = 0)$	126.405501	126.405135	3×10^{-6}
$h_{\text{PNC}} (\omega = 0)$	-1.0700928	-1.0700932	4×10^{-7}

$$^* \epsilon \equiv (lhs - rhs) / lhs$$

where w is the Wronskian (21), and S is the rhs of Eq. (60) (the $\delta\varepsilon$ term only contributes for the X term with $\alpha = a$). The $X_\alpha^{0,\infty}$ orbitals here are the solutions with Dirac quantum number α to the homogenous equation (20). We defined here the “partial” matrix elements, that include only the integral over angular coordinates:

$$\{\psi_a | \hat{h} | \psi_b\} \equiv \int \psi_a^\dagger \hat{h} \psi_b d\Omega. \quad (62)$$

We similarly define the partial reduced matrix element:

$$\{\psi_a | T_q^k | \psi_b\} \equiv (-1)^{j_a-m_a} \begin{pmatrix} j_a & k & j_b \\ -m_a & q & m_b \end{pmatrix} \{\psi_a || T^k || \psi_b\}. \quad (63)$$

Then, in terms of the partial waves (χ), the solution becomes:

$$\chi_\alpha = \frac{\chi_\alpha^\infty}{cw} \int_0^r \{\chi_\alpha^0 | S\} r^2 dr' + \frac{\chi_\alpha^0}{cw} \int_r^\infty \{\chi_\alpha^\infty | S\} r^2 dr'. \quad (64)$$

This is done so that we only need to calculate the (m -independent) reduced matrix element of \hat{h} . The radial integral $|\chi_\alpha|^2$ is used to control convergence (for including the exchange term). Using U_x from Sec. 3.4, convergence (for a given orbital) to parts in 10^9 is typically reached in ~ 10 iterations.

One may use the perturbation expression (57) to test the method. Consider, e.g., (excluding δV)

$$\langle m | \chi \rangle = \frac{\langle m | \hat{h} | \psi \rangle}{\varepsilon - \varepsilon_m + \omega}, \quad (65)$$

which can be calculated both ways (lhs vs rhs); see Table 3.

An important application of this technique is that it allows calculations to be done without requiring a summation over the complete set of intermediate states (replaced by solving the inhomogeneous differential equation). This method of performing exact summation over intermediate states is sometimes called the Solving Equations, Mixed States, or Dalgarno-Lewis method [13], depending on context. In this example (65) the intermediate-states summation is trivial, since it involves only single operator and hence only a single intermediate state contributes. In general, all intermediate states (including continuum and positive energy states) contribute, so this method allows calculations without the need for a large basis.

Another way to test the method is to consider the parity non-conservation (PNC) amplitude, which is a correction to the (otherwise forbidden) $E1$ transition between states of the same parity, due to the parity-violating weak interaction between the electrons and nucleus (see, e.g., Ref. [14]). This can be expressed as a sum over all intermediate states n :

$$E_{\text{PNC}}^{(z)} = \sum_n \frac{\langle B | \mathbf{d}_z | n \rangle \langle n | h_W | A \rangle}{\varepsilon_A - \varepsilon_n} + \frac{\langle B | h_W | n \rangle \langle n | \mathbf{d}_z | A \rangle}{\varepsilon_B - \varepsilon_n}, \quad (66)$$

where \mathbf{d} is the $E1$ operator, and h_W is the PNC operator. Using the TDHF (Dalgarno-Lewis) method as described in Sec. 5.1,

Table 4: Comparison of PNC amplitudes (at the HF level) for ^{133}Cs as calculated using the TDHF method, and direct summation using a spline basis [in a cavity of $(10^{-6}, 50) a_B$ using N splines of order k].

Transition	TDHF	Direct Summation: N/k		
		50/5	60/6	70/7
$6s - 7s$	-0.73954	-0.73948	-0.73953	-0.73954
$6s - 5d_{3/2}$	-2.4000	-2.3998	-2.4000	-2.4000

this can also be expressed in two other formally equivalent ways:

$$E_{\text{PNC}}^{(z)} = \langle B | \mathbf{d}_z | \delta A^{(W)} \rangle + \langle \delta B^{(W)} | \mathbf{d}_z | A \rangle \quad (67)$$

$$= \langle \delta B^{(d)} | h_W | A \rangle + \langle B | h_W | \delta A^{(d)} \rangle, \quad (68)$$

where $\delta A^{(W/d)}$ is the correction to orbital A due to the weak/EI interaction. Comparing the results of Eqs. (67) and (68) tests the numerical accuracy of the Dalgarno Lewis (solving-equations) method, and comparing these to the result of (66) gives a good test of the basis. The two forms of the Dalgarno Lewis method agree to parts in 10^8 . Comparison between the PNC amplitude as calculated using this and the direct-summation method is in Table 4.

5.3 Core polarisation (RPA)¹⁶

This section largely follows Ref. [12] (see also [15–18]). In the presence of an external field, the core electrons become perturbed (54), and a correction to the HF potential is induced. This leads to important corrections to the matrix elements of the external field operator. This effect is often called core polarisation, and is particularly important since it involves corrections with single excitations from the HF core (in the absence of an external field, the lowest-order corrections to the HF potential involve double excitations). The method described here is often referred to as the random phase approximation (RPA).

To account for core polarisation, the set of TDHF equations (55) are solved self-consistently for each of the core orbitals (see Sec. 5.1). The δV term is the correction to the HF potential:

$$\delta V = V_{\text{HF}}(\{\psi_b + \delta\psi^b\}) - V_{\text{HF}}(\{\psi_b\}), \quad (69)$$

where $\{\psi_b\}$ denotes the set of all core orbitals.

The TDHF equations are solved iteratively, updating the δV and $\delta\varepsilon$ terms at each step until convergence is reached; i.e., at the n th step, we have

$$(h_{\text{HF}} - \varepsilon - \omega) X_{\beta}^{(n)} = - \left(\hat{h} + \delta V^{(n-1)} - \delta\varepsilon^{(n-1)} \right) \psi_b, \quad (70)$$

with $\delta V = 0$ for the initial iteration (similarly for Y). The $\delta\varepsilon$ term only survives in the equations when $\beta = b$ [see Eq. (61)].

Combining Eqs. (69) with (54), (56), and (29), we have:

$$\begin{aligned} \delta V \phi_a(\mathbf{r}_1) = & \sum_{i \neq a}^{N_c} \int \frac{d^3 \mathbf{r}_2}{|\mathbf{r}_{12}|} \left(\phi_i^{\dagger}(\mathbf{r}_2) [X^i(\mathbf{r}_2) \phi_a(\mathbf{r}_1) - \phi_a(\mathbf{r}_2) X^i(\mathbf{r}_1)] \right. \\ & \left. + Y^{i\dagger}(\mathbf{r}_2) [\phi_i(\mathbf{r}_2) \phi_a(\mathbf{r}_1) - \phi_a(\mathbf{r}_2) \phi_i(\mathbf{r}_1)] \right). \end{aligned} \quad (71)$$

The reduced matrix elements of δV are:

$$\langle \phi_n || \delta V || \phi_a \rangle = \sum_{b\beta} \frac{(-1)^{j_n + j_\beta + k + 1}}{[k]} (W_{nba\beta}^k + W_{n\beta'ab}^k), \quad (72)$$

¹⁶Implemented: /src/ExternalField/CorePolarisation.hpp, TDHF.hpp

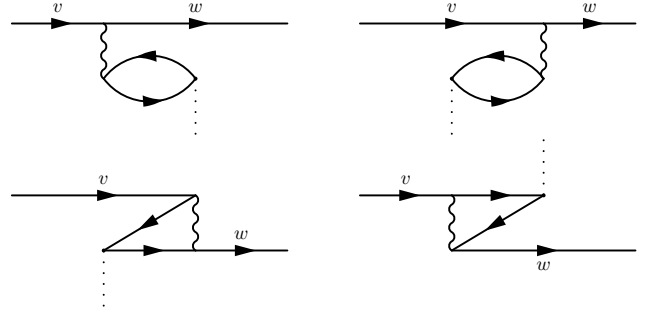


Figure 4: Diagrams representing the lowest order direct and exchange core-polarisation (RPA) corrections to the $\langle w | \hat{h} | v \rangle$ amplitude. Wavy line is Coulomb interaction, dotted line is external field (\hat{h}). All internal lines are summed over: forwards lines are virtual excited states, backward lines are holes in the core. In higher-order diagrams, each \hat{h} vertex is corrected again by these four diagrams (RPA).

where we define reduced Coulomb integrals (see Appendix A.4):

$$W_{abcd}^k \equiv Q_{abcd}^k + [k] \sum_{\lambda} \left\{ \begin{matrix} j_a & j_c & k \\ j_b & j_d & \lambda \end{matrix} \right\} Q_{abdc}^{\lambda}, \quad (73)$$

$$Q_{abcd}^k \equiv (-1)^{j_a + j_b + k + 1} C_{ac}^k C_{bd}^k R_{abcd}^k, \quad (74)$$

$$R_{abcd}^k \equiv \int d\mathbf{r}_1 [f_a(r_1) f_c(r_1) + g_a(r_1) g_c(r_1)] y_{bd}^k(r_1), \quad (75)$$

with y_{bd}^k and C_{ab}^k given by Eqs. (32) and (33).¹⁷ The sum b runs over core orbitals, and β runs over all corrections to b [Eq. (56)]. The prime (β') means the η_{β} orbital is used; no prime means χ_{β} . The equation for $\langle \phi_n || \delta V^{\dagger} || \phi_a \rangle$ is the same, but with $\beta \leftrightarrow \beta'$.

The amplitude for a transition from state $v \rightarrow w$ in the TDHF method can be found from analogy with regular time-dependent perturbation theory (e.g., [19]), where

$$\delta\psi_v(t) \simeq \frac{M_{wv}}{\varepsilon_v - \varepsilon_w + \omega} \psi_b e^{-i\omega t}$$

(keeping only the resonant term with $\omega \approx \varepsilon_v - \varepsilon_w$). At the same time, from Eq. (55), we have

$$\langle \psi_w | \delta\psi_v(t) \rangle = \langle \psi_w | X^v \rangle e^{-i\omega t} = \frac{\langle \psi_w | \hat{h} + \delta V | \psi_v \rangle}{\varepsilon_v - \varepsilon_w + \omega} e^{-i\omega t}. \quad (76)$$

Combining leads to the expression:

$$M_{wv} = \langle w | \hat{h} + \delta V | v \rangle. \quad (77)$$

Since δV was found self-consistently, the matrix elements include core polarisation to all-orders [12, 20]. This is equivalent to the RPA method (see, e.g., Ref. [3]). If the equations (70) are solved just once (without iterations), it corresponds to the lowest (first) order correction to the amplitude, which are shown in Fig. 4. Further iterations correspond to higher-orders.

5.4 Core polarisation (RPA diagram technique)¹⁸

The core polarisation correction to a matrix element can also be taken into account by directly evaluating the four diagrams in Fig. 4. To lowest order, the matrix element of operator \hat{h} is $h_{ij}^{(0)}$. The first-order correction is then [2]:

$$\delta h_{ij} = \sum_{ma} \frac{h_{am}^{(0)} \tilde{g}_{imja}}{\varepsilon_a - \varepsilon_m - \omega} + \sum_{ma} \frac{h_{ma}^{(0)} \tilde{g}_{iajm}}{\varepsilon_a - \varepsilon_m + \omega}, \quad (78)$$

¹⁷Note: Q^k here differs from that defined in, e.g., Ref. [12] by a factor of ± 1 ; our definition is chosen due to the symmetry properties; see A.4.

¹⁸Implemented in: /src/ExternalField/DiagramRPA.hpp

where $\tilde{g}_{abcd} = g_{abcd} - g_{abdc}$, with g_{abcd} being the two-electron Coulomb matrix element (see appendix for definition). The a sum runs over all occupied core electrons (n, κ, m), while m runs over all virtual excited states.

In the RPA method, the lowest-order matrix elements in δh_{ij} (78) are then replaced with the corrected values. This process is repeated iteratively (for all core states i and j) until convergence is reached; i.e., at the n th iteration we have:

$$\delta h_{ij}^n = \sum_{ma} \left(\frac{(h_{am}^{(0)} + \delta h_{am}^{n-1}) \tilde{g}_{imja}}{\varepsilon_a - \varepsilon_m - \omega} + \frac{(h_{ma}^{(0)} + \delta h_{ma}^{n-1}) \tilde{g}_{iajm}}{\varepsilon_a - \varepsilon_m + \omega} \right). \quad (79)$$

The reduced matrix element in the RPA approach is then:

$$\langle i || h || j \rangle^{\text{RPA}} = \langle i || h || j \rangle + \langle i || \delta h || j \rangle, \quad (80)$$

with

$$\langle i || \delta h || j \rangle = \frac{1}{[k]} \sum_{am} (-1)^{j_a - j_i + k} \left(\frac{\langle a || h || m \rangle^{\text{RPA}} W_{imja}^k}{\varepsilon_a - \varepsilon_m - \omega} + (-1)^{j_a - j_m} \frac{\langle m || h || a \rangle^{\text{RPA}} W_{iajm}^k}{\varepsilon_a - \varepsilon_m + \omega} \right), \quad (81)$$

(sum is now over orbitals n, κ). RPA matrix elements between valence states have the same expression (the equations need only be iterated for the core electrons). Note that W depends only on the *rank* of the operator, so in theory, they need only be calculated once. In practise, we only calculate W_{imja}^k when $h_{am} \neq 0$, meaning effectively that W also depends on the operator parity. It can be shown the diagram and TDHF methods are equivalent: $\langle i || \delta h || j \rangle = \langle i || \delta V || j \rangle$ [see Eq. (57)].

5.5 Core polarisation (“basis” technique)¹⁹

Sometimes, the TDHF equations do not converge due to instabilities in solving the mixed-states equations (55). There are several ways to proceed in these cases, including using the diagram method as above, and using algebraic (matrix) techniques [18]. We also implement a method where the TDHF equations are solved using perturbation theory, by expanding the χ and η functions over a basis using Eq. (57). (Note that, unlike the matrix technique, this required iterations since the expansion depends on δV .) Then, δV remains as Eq. (72). This allows inclusion of the Breit effect into δV (see Sec. 10.1) (which are not so simple to include in the diagram method).

6 Correlation corrections²⁰

Correlation corrections are the deviation from the pure single-particle picture, and correspond to many-body effects beyond the mean field (Hartree-Fock) approximation. The many-body atomic Hamiltonian may be expressed as

$$H = \sum_i h_{\text{HF}}(\mathbf{r}_i) + \delta V_{\text{corr}}, \quad (82)$$

where $h_{\text{HF}}(\mathbf{r}_i)$ is the single-particle HF Hamiltonian (28), and

$$\delta V_{\text{corr}} = \sum_{i < j} \frac{1}{\mathbf{r}_{ij}} - \sum_i V_{\text{HF}}(\mathbf{r}_i) \quad (83)$$

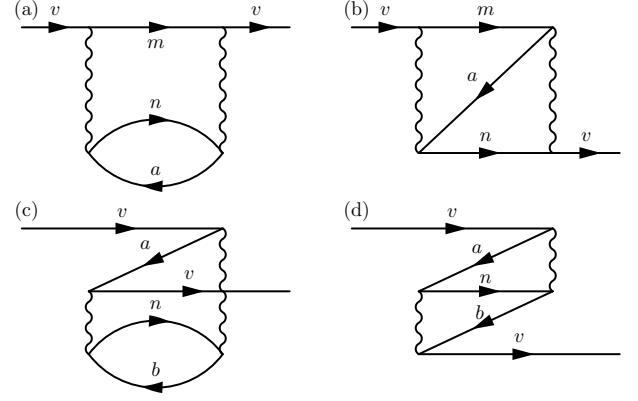


Figure 5: Goldstone diagrams for the second-order correlation correction to the energy for valence state v . Backward facing lines denote (single-particle) states in the core; n and m are virtual excited states. Diagrams (a) and (c) are direct diagrams, (b) and (d) are corresponding exchange diagrams.

is the *residual Coulomb interaction* (beyond the mean potential) that may be taken into account perturbatively. We consider the case of an atom with a single valence electron (v) above closed shells. In the single particle picture, this perturbation corresponds to residual interactions of the valence electron with the individual electrons in the core. Starting from the Hartree-Fock method with a V^{N-1} potential, there are no first-order corrections to the wavefunction (that is, corrections involving a single core excitation) [2].

Notation: I use the convention that letters at the beginning of the alphabet (a, b, \dots) denote occupied core states (or holes), those from the middle (n, m, \dots) denote virtual excited states, and those from the end (v, w, \dots) denote valence states. The letters (i, j, \dots) are dummy indices that may stand for any state.

6.1 Second-order correlations: Goldstone technique

This section follows closely the method from Ref. [12]. Goldstone diagrams for the second-order correction to the valence energy are shown in Fig. 5. This can be expressed as [3, 12]:

$$\delta E_v = \sum_{amn} \frac{g_{vamn} \tilde{g}_{nmav}}{\varepsilon_v + \varepsilon_a - \varepsilon_m - \varepsilon_n} + \sum_{abn} \frac{g_{vnab} \tilde{g}_{banv}}{\varepsilon_v + \varepsilon_n - \varepsilon_a - \varepsilon_b}, \quad (84)$$

where m and n run over (unoccupied) virtual excited states, and a and b run over (occupied) core states (there is an implicit sum over magnetic quantum numbers here). The first term corresponds to the diagrams (a) and (b), the second to (c) and (d) [Fig. 5]. Here, $\tilde{g}_{abcd} = g_{abcd} - g_{abdc}$ is the anti-symmetrised integral (accounting for exchange; see appendix), with

$$g_{abcd} = \sum_{kq} (-1)^q \langle a_{\kappa m} | C_{-q}^k | c_{\kappa m} \rangle \langle b_{\kappa m} | C_q^k | d_{\kappa m} \rangle R_{abcd}^k. \quad (85)$$

Summing over magnetic quantum numbers, this gives [12]

$$\delta E_v = \sum_k \frac{1}{[k][j_v]} \left(\sum_{amn} \frac{Q_{vamn}^k W_{vamn}^k}{\varepsilon_v + \varepsilon_a - \varepsilon_m - \varepsilon_n} + \sum_{abn} \frac{Q_{vnba}^k W_{vnba}^k}{\varepsilon_v + \varepsilon_n - \varepsilon_b - \varepsilon_a} \right), \quad (86)$$

where Q^k, W^k and are given by Eqs. (74), (73), and we used the symmetries and angular identities given in Appendix A.4.

¹⁹Implemented in: /src/ExternalField/TDHFbasis.hpp

²⁰Implemented in: /src/MBPT/CorrelationPotential.hpp

We define the *correlation potential*, $\hat{\Sigma}$, so that its matrix elements correspond to the energy shift: $\langle v | \Sigma^{(2)} | v \rangle = \delta E_v$. We define $Q_{nba}^{k(\kappa_v)}(r)$ (which we will write as $Q_{nba}^{k(v)}$ for brevity, though note it depends only on κ_v and not F_v), via:

$$Q_{v nba}^k = \langle F_v | Q_{nba}^{k(v)} \rangle = \int F_v(r) Q_{nba}^{k(v)}(r) dr. \quad (87)$$

Note that $Q_{nba}^{k(v)}$ has the form of a radial Dirac spinor [Eq. (8)]. Then, we may express the (energy dependent) second-order correlation potential as

$$\hat{\Sigma}_\varepsilon^{(2)} = \sum_k \frac{1}{[k][j_v]} \left(\sum_{amn} \frac{|Q_{amn}^{k(v)}\rangle \langle W_{amn}^{k(v)}|}{\varepsilon + \varepsilon_a - \varepsilon_m - \varepsilon_n} + \sum_{abn} \frac{|Q_{nba}^{k(v)}\rangle \langle W_{nba}^{k(v)}|}{\varepsilon + \varepsilon_n - \varepsilon_b - \varepsilon_a} \right), \quad (88)$$

which is sometimes called the self-energy operator. This has the form of a sum of operators,

$$\hat{G}_{nba}^{(v)}(\varepsilon) = \sum_k \frac{1}{[k][j_v]} \frac{|Q_{nba}^{k(v)}\rangle \langle W_{nba}^{k(v)}|}{\varepsilon + \varepsilon_n - \varepsilon_b - \varepsilon_a}, \quad (89)$$

which can be expressed in (radial) coordinate space as

$$G_{nba}^{(v)}(r_1, r_2, \varepsilon) = \sum_k \frac{1}{[k][j_v]} \frac{Q_{nba}^{k(v)}(r_1) W_{nba}^{k(v)}(r_2)}{\varepsilon + \varepsilon_n - \varepsilon_b - \varepsilon_a}. \quad (90)$$

Thus the correlation potential may be expressed as

$$\Sigma_\varepsilon^{(2)}(r_1, r_2) = \sum_{abnm} \left[G_{amn}^{(v)}(r_1, r_2, \varepsilon) + G_{nba}^{(v)}(r_1, r_2, \varepsilon) \right]. \quad (91)$$

Note that Σ is a matrix in (radial) spinor space:

$$\Sigma \propto \begin{pmatrix} f_Q(r_1) f_W(r_2) & f_Q(r_1) g_W(r_2) \\ g_Q(r_1) f_W(r_2) & g_Q(r_1) g_W(r_2) \end{pmatrix}, \quad (92)$$

where f and g are the large and small components of the Q/W radial spinors. Each of these four terms can themselves be represented as square matrices (on a radial grid). It is common to only calculate the first (ff) term; it is also common to store the Σ matrix on only a subset of the radial grid.

6.2 Correlation potential method (Brueckner orbitals)

In the *correlation potential method* [22, 23], the non-local energy-dependent Σ operator is added to the single-particle Hartree-Fock equation for the valence states:

$$(h_{\text{HF}} + \hat{\Sigma}_\varepsilon) \psi^{(\text{Br})} = \varepsilon^{(\text{Br})} \psi^{(\text{Br})}. \quad (93)$$

The resulting orbitals, known as Brueckner orbitals²¹, include the second-order correlation effects. This means, for example, the dominant correlation corrections can be included into the calculation of matrix elements simply by using the Brueckner orbitals, e.g., $\langle a^{\text{HF}} | \hat{v} | b^{\text{HF}} \rangle \rightarrow \langle a^{\text{Br}} | \hat{v} | b^{\text{Br}} \rangle$. We will drop the (Br) superscript from here on unless it is necessary to avoid confusion. The iterations of the Hartree-Fock equation for the valence state actually means that certain classes of diagrams are included to all orders; this is called the *chainning* of the self-energy operator. Calculations using the second-order correlation potential

²¹Note that the exact definition of “Brueckner” orbitals varies slightly depending on the source; we use the definition from [22].

method for energies of the lowest states of the alkali atoms are presented in Table 5.

The Σ operator should be evaluated at the Hartree-Fock energy of the valence state. The correlation potential depends only weakly on ε_v [see Eq. (86)], so it is often instead found at the energy of the lowest valence state v of the given symmetry (since this is typically where the highest accuracy is required, and because the correlation corrections are larger for lower states).

One may also include the correlation corrections into a set of basis orbitals by adding the correlation potential to the Hartree-Fock Hamiltonian when solving the eigenvalue problem for the set of B-splines; i.e.,

$$h_{ij} \rightarrow \langle S_i | \hat{h}_{\text{HF}} | S_j \rangle + \langle S_i | \hat{\Sigma}_\varepsilon | S_j \rangle \quad (94)$$

in Eq. (51). This leads to an (approximately) complete set of orbitals that include correlation effects. These orbitals may then be used in calculations requiring a summation of a complete set of orbitals; so this method allows the inclusion of correlation corrections into such calculations in a reasonably simple way.

The correlation potential can also be taken into account in the time-dependent Hartree-Fock method for the valence state:

$$\left(h_{\text{HF}} + \hat{\Sigma}_\varepsilon - \varepsilon - \omega \right) X = - \left(\hat{h} + \delta V - \delta \varepsilon \right) \psi_v. \quad (95)$$

This gives a means of including the correlation corrections into the Dalgarno-Lewis (Mixed-States) method.

7 Correlation potential: Feynman method

In the previous section, I described the usual second-order many-body perturbation theory method using the Goldstone diagram technique. Here, I outline an alternative approach: the Feynman method. This method does not require a summation over intermediate states (i.e., no basis is required), but instead introduces an integral over frequencies. Importantly, the Feynman method allows several classes of dominating higher-order corrections (Coulomb screening and the hole-particle interaction) to be included to all-orders by an exact summation of series of diagrams. This section describes the method as developed in Ref. [24], and follows that work closely; see also [25–27].

In this section, I will sometimes include subscripts on the Dirac bra/kets to indicate which coordinate they belong to. I will also abuse the Dirac notation here so that $|a\rangle_1$ is just a short-hand for $\phi_a(\mathbf{r}_1)$; note that when the coordinate index is shown, there is no implied integration in the bracket, e.g.:

$$\langle a|_1|b\rangle_1 = \phi_a^\dagger(\mathbf{r}_1)\phi_b(\mathbf{r}_1), \quad \text{while} \quad \langle a|b\rangle = \int d^3\mathbf{r}' \phi_a^\dagger(\mathbf{r}')\phi_b(\mathbf{r}').$$

7.1 Feynman Green’s function

First, we introduce the Feynman Green’s function, which can be expressed as (see [24, 25] and references therein):

$$\hat{G}(\varepsilon) = \lim_{\delta \rightarrow 0} \left(\sum_a^{\text{core}} \frac{|a\rangle \langle a|}{\varepsilon - \varepsilon_a - i\delta} + \sum_n^{\text{exc.}} \frac{|n\rangle \langle n|}{\varepsilon - \varepsilon_n + i\delta} \right). \quad (96)$$

Note that, if ε is the (single-particle) ground-state energy, $\varepsilon > \varepsilon_a$, but $\varepsilon < \varepsilon_n$. Conceptually, the simplest way to evaluate it is by summation over the complete set of core and excited orbitals using a pseudospectrum basis as described previously. It is also, however, possible to evaluate the Green’s function exactly (up to numerical errors) without the need for a basis.

Table 5: Removal energies for the lowest s , p , and d states for the alkali atoms as calculated with the Hartree-Fock and second-order correlation potential methods, and comparison with experiment (Ref. [21]). Note: Calculation of Σ used only basis states up to $l = 4$; states up to $l = 6$ are important, especially for heavy atoms, so these should be taken as an example only. The inclusion of the correlation potential greatly improves the accuracy of the calculations.

Expt.						HF		$\Sigma^{(2)}$		Expt.						HF		$\Sigma^{(2)}$											
Li ($Z = 3$)										Rb ($Z = 37$)																			
$2s_{1/2}$	-43487.1	-43087.3	-0.9%	-43450.6	-0.08%	$5s_{1/2}$	-33690.8	-30570.9	-9.3%	-34162.9	1.4%	$5p_{1/2}$	-21111.9	-19931.8	-5.6%	-21231.3	0.6%	$5p_{3/2}$	-20874.3	-19749.6	-5.4%	-20982.4	0.5%						
$2p_{1/2}$	-28583.5	-28232.9	-1.2%	-28539.3	-0.15%	$4d_{3/2}$	-14335.6	-13112.5	-8.5%	-14415.9	0.6%	$4d_{5/2}$	-14335.2	-13099.7	-8.6%	-14411.7	0.5%												
$2p_{3/2}$	-28583.1	-28232.3	-1.2%	-28538.7	-0.16%																								
$3d_{3/2}$	-12204.0	-12194.4	-0.08%	-12208.3	0.04%																								
$3d_{5/2}$	-12204.0	-12194.4	-0.08%	-12208.3	0.04%																								
Na ($Z = 11$)						Cs ($Z = 55$)																							
$3s_{1/2}$	-41449.5	-39951.5	-3.6%	-41272.7	-0.4%	$6s_{1/2}$	-31406.5	-27954.1	-11.0%	-32289.8	2.8%	$6p_{1/2}$	-20228.2	-18790.5	-7.1%	-20488.3	1.3%	$6p_{3/2}$	-19674.2	-18388.8	-6.5%	-19894.6	1.1%	$5d_{5/2}$	-16907.2	-14162.6	-16.2%	-17230.9	1.9%
$3p_{1/2}$	-24493.3	-24030.4	-1.9%	-24427.8	-0.3%	$5d_{3/2}$	-16809.6	-14138.5	-15.9%	-17090.5	1.7%																		
$3p_{3/2}$	-24476.1	-24014.1	-1.9%	-24409.6	-0.3%																								
$3d_{5/2}$	-12276.6	-12217.4	-0.5%	-12267.5	-0.07%																								
$3d_{3/2}$	-12276.6	-12217.4	-0.5%	-12267.4	-0.07%																								
K ($Z = 19$)						Fr ($Z = 87$)																							
$4s_{1/2}$	-35009.8	-32370.4	-7.5%	-35316.2	0.9%	$7s_{1/2}$	-32848.9	-28767.1	-12.4%	-33944.4	3.3%	$7p_{1/2}$	-20611.5	-18855.2	-8.5%	-20928.5	1.5%	$7p_{3/2}$	-18924.9	-17655.3	-6.7%	-19124.5	1.1%	$6d_{3/2}$	-16619.0	-13924.5	-16.2%	-16872.6	1.5%
$4p_{1/2}$	-22024.6	-21006.5	-4.6%	-22097.1	0.3%	$6d_{5/2}$	-16419.2	-13825.5	-15.8%																				
$4p_{3/2}$	-21966.9	-20959.4	-4.6%	-22036.1	0.3%																								
$3d_{5/2}$	-13475.1	-12747.0	-5.4%	-13516.3	0.3%																								
$3d_{3/2}$	-13472.8	-12744.3	-5.4%	-13514.6	0.3%																								

Consider the inhomogeneous Hartree-Fock equation including the direct (V_d) and exchange (V_x) potentials, and its homogeneous counterpart (without exchange):

$$(h_0 + V_d - \varepsilon)\phi = -V_x\phi \quad (97)$$

$$(h_0 + V_d - \varepsilon)\chi = 0, \quad (98)$$

with χ_0 being the homogeneous solution regular at the origin, and χ_∞ that regular at infinity. The local Green's function (without exchange) can be expressed in coordinate space as:

$$\hat{G}_0 \equiv G_0(\mathbf{r}_1, \mathbf{r}_2) = \frac{\chi_0(r_<, \hat{\mathbf{n}})\chi_\infty(r_>, \hat{\mathbf{n}})}{w}, \quad (99)$$

where $r_< = \min(r_1, r_2)$, and $w = (f_0g_\infty - f_\infty g_0)/\alpha$ (w is independent of r , and f, g are radial components of χ). Exchange can be taken into account by solving the Dyson equation [25, 26]

$$\hat{G} = \hat{G}_0 + \hat{G}_0 \hat{V}_x \hat{G} = \left[1 - \hat{G}_0 \hat{V}_x\right]^{-1} \hat{G}_0. \quad (100)$$

The local direct and non-local exchange operators are

$$\hat{V}_d = \sum_a^{\text{core}} \langle a | \hat{Q} | a \rangle, \quad \text{and} \quad \hat{V}_x = - \sum_a^{\text{core}} | a \rangle \hat{Q} \langle a |, \quad (101)$$

respectively, with the (two-particle) Coulomb operator:

$$\hat{Q}(\mathbf{r}_1, \mathbf{r}_2) = \mathbf{r}_{12}^{-1}. \quad (102)$$

These operators may be represented as coordinate matrices: e.g., $\hat{G} \Leftrightarrow G(\mathbf{r}_1, \mathbf{r}_2)$. Multiplication is understood to mean:

$$\hat{W} = \hat{X} \hat{Y} \hat{Z} \Rightarrow W(r_1, r_2) = \iint dr_i dr_j X(r_1, r_i) Y(r_i, r_j) Z(r_j, r_2).$$

Note that G, Q, V etc. are symmetric.

7.2 Two useful integrals

Here, I present two useful analytic integrals involving Feynman Green's functions. These are evaluated analytically by extending the integral over the complex plane. As a reminder, Cauchy's

integral formula is

$$\oint dz \frac{f(z)}{z - a} = 2\pi i f(a).$$

The first integral²²

$$\int \frac{d\omega}{2\pi} \hat{G}_{12}(\varepsilon_i + \omega) \hat{G}_{34}(\varepsilon_j + \omega) \quad (103)$$

$$= \sum_{abnm} \int \frac{d\omega}{2\pi} \left(\frac{|a\rangle_1 \langle a|_2}{\varepsilon_i + \omega - \varepsilon_a - i\delta} + \frac{|n\rangle_1 \langle n|_2}{\varepsilon_i + \omega - \varepsilon_n + i\delta} \right) \times \left(\frac{|b\rangle_3 \langle b|_4}{\varepsilon_j + \omega - \varepsilon_b - i\delta} + \frac{|m\rangle_3 \langle m|_4}{\varepsilon_j + \omega - \varepsilon_m + i\delta} \right), \quad (104)$$

can be expanded to four separate terms, each with a pair of poles. Consider the first (“ a, b ”) term of (104):

$$\int \frac{d\omega}{2\pi} \left(\frac{|a\rangle \langle a|}{\varepsilon_i + \omega - \varepsilon_a - i\delta} \right) \left(\frac{|b\rangle \langle b|}{\varepsilon_j + \omega - \varepsilon_b - i\delta} \right), \quad (105)$$

which has poles at $\omega = \varepsilon_{a/b} - \varepsilon_{i/j} + i\delta$. By closing the contour in the lower complex plane (Fig. 6, left), it is seen the integral is zero. The same is found for the last (“ n, m ”) term by closing in the upper plane. The other two terms are non-zero, and can be evaluated by closing in (e.g.) the upper plane; an example for the “ a, m ” term with pole at $\omega = \varepsilon_a - \varepsilon_i + i\delta$ is given in Fig. 6 (right). Together, this gives the final expression:²³

$$\int \frac{d\omega}{2\pi} \hat{G}_{12}(\varepsilon_i + \omega) \hat{G}_{34}(\varepsilon_j + \omega) = i \sum_{an} \left[\frac{|a\rangle_1 \langle a|_2 |n\rangle_3 \langle n|_4}{\varepsilon_j - \varepsilon_i + \varepsilon_a - \varepsilon_n} + \frac{|n\rangle_1 \langle n|_2 |a\rangle_3 \langle a|_4}{\varepsilon_i - \varepsilon_j + \varepsilon_a - \varepsilon_n} \right]. \quad (106)$$

The second integral is found in the same way:

$$\int \frac{d\omega}{2\pi} \hat{G}_{12}(\varepsilon_i + \omega) \hat{G}_{34}(\varepsilon_j - \omega) = i \sum_{abnm} \left[\frac{|a\rangle_1 \langle a|_2 |b\rangle_3 \langle b|_4}{\varepsilon_i + \varepsilon_j - \varepsilon_a - \varepsilon_b} - \frac{|n\rangle_1 \langle n|_2 |m\rangle_3 \langle m|_4}{\varepsilon_i + \varepsilon_j - \varepsilon_m - \varepsilon_n} \right]. \quad (107)$$

²²Note $|G(\omega)| \rightarrow 0$ as $|\omega| \rightarrow \infty$ ($\omega \in \mathbb{C}$); see Eq. (96).

²³I renamed $m = n$ in the first term, and $b = a$ in the second.

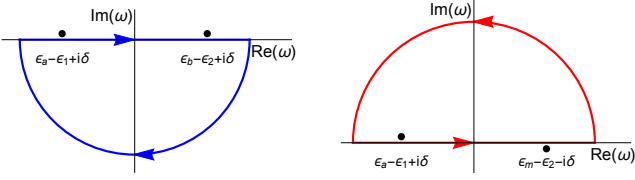
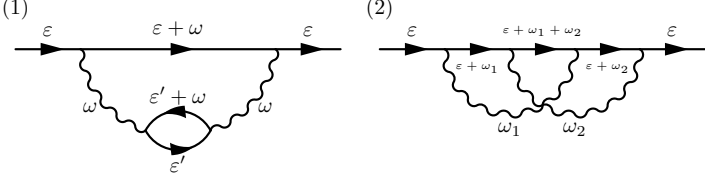

 Figure 6: Contours for the “ a, b ” and “ a, m ” terms of Eq. (104).


Figure 7: Second-order direct (1) and exchange (2) correlation diagrams in the Feynman technique. The straight lines represent Hartree-Fock (bound-electron) Green’s functions (96), the wavy photon lines represent the (non-relativistic) Coulomb operator (102).

7.3 Feynman method for second-order correlations

The second-order correlation corrections are given by the diagrams presented in Fig. 7. The electron loop in Fig. 7 (1) may be written in terms of the polarisation operator:

$$\hat{\Pi}_{12}(\omega) = \int \frac{d\varepsilon'}{2\pi} \hat{G}_{12}(\varepsilon') \hat{G}_{21}(\omega + \varepsilon'). \quad (108)$$

Note that this is a (largely) non-relativistic many-body problem; the polarisation is of the atomic core, not the vacuum, and relativistic corrections to the Coulomb operator can be excluded (see Breit and QED corrections discussed later). In this formalism, Feynman diagrams carry a phase factor of

$$i^{N_Q} (-1)^{N_l}, \quad (109)$$

where N_Q is the number of Coulomb (wavy) lines, and N_l is the number of closed loops.

Using Eq. (106), the integral over frequencies in the polarisation operator can be performed analytically, yielding:

$$\hat{\Pi}(\omega) = i \sum_{an} \left[\frac{|a\rangle_2 \langle a|_1 |n\rangle_1 \langle n|_2}{\varepsilon_a - \omega - \varepsilon_n} + \frac{|n\rangle_2 \langle n|_1 |a\rangle_1 \langle a|_2}{\varepsilon_a + \omega - \varepsilon_n} \right], \quad (110)$$

which can be further simplified to:

$$\hat{\Pi}(\omega) = i \sum_a |a\rangle \left[\hat{G}^{\text{ex}}(\varepsilon_a - \omega) + \hat{G}^{\text{ex}}(\varepsilon_a + \omega) \right] \langle a|. \quad (111)$$

Here, $\hat{G}^{\text{ex}} \equiv \hat{G} - \hat{G}^{\text{core}}$ only includes excited orbitals, and may be formed without the use of a basis using Eqs. (100) and (96), so long as the core orbitals are known. It is more numerically stable to calculate it as:

$$\hat{G}^{\text{ex}} = \hat{G} - \sum_a^{\text{core}} |a\rangle \langle a| \hat{G}. \quad (112)$$

With these, the direct (d) and exchange (x) correlation potentials can be expressed in the Feynman approach as

$$\hat{\Sigma}_d^{(2)} = \iint d^3r_i d^3r_j \int \frac{d\omega}{2\pi} \hat{G}_{12}(\varepsilon + \omega) \hat{Q}_{1i} \hat{\Pi}_{ij}(\omega) \hat{Q}_{j2}, \quad (113)$$

and

$$\hat{\Sigma}_x^{(2)} = - \iint d^3r_i d^3r_j \iint \frac{d\omega_1}{2\pi} \frac{d\omega_2}{2\pi} \hat{G}_{1i}(\varepsilon + \omega_1) \hat{Q}_{1j} \hat{G}_{ij}(\varepsilon + \omega_1 + \omega_2) \hat{Q}_{i2} \hat{G}_{j2}(\varepsilon + \omega_2). \quad (114)$$

Table 6: Expectation values of the direct part of the correlation potential $\langle v | \Sigma_d | v \rangle$ for the lowest valence states of Cs (atomic units). The first four rows correspond to the second-order Goldstone technique using various number of states in the MBPT expansion, and the fifth row is the second-order Feynman technique. The final two rows are the screening and hole-particle corrections (see below).

	6s _{1/2}	6p _{1/2}	6p _{3/2}	5d _{3/2}	5d _{5/2}
30spdfghi	-0.01906	-0.00771	-0.00693	-0.01226	-0.01182
40spdfghi	-0.01915	-0.00768	-0.00690	-0.01228	-0.01182
50spdfghi	-0.01919	-0.00769	-0.00691	-0.01230	-0.01184
60spdfghi	-0.01920	-0.00769	-0.00691	-0.01230	-0.01184
Feynman	-0.01920	-0.00766	-0.00689	-0.01236	-0.01190
δScreen	0.00631	0.00246	0.00221	0.00331	0.00313
δh-p	-0.00769	-0.00359	-0.00322	-0.00477	-0.00457

The signs are due to Eq. (109). In the Feynman technique, as compared to the Goldstone technique, we avoid the need for a summation over the complete set of states, but instead require integration over frequencies. Note that $\Sigma = \Sigma_d + \Sigma_x$ is also called the self-energy operator. Comparison between the Feynman and Goldstone corrections shown in Table 6. Note that the Feynman direct diagram is calculated *much* faster than the Goldstone one when a large basis is required

7.4 Feynman to Goldstone transformation

Here, we show the connection between the Feynman and Goldstone approaches, by demonstrating the Feynman expressions reduce to the Goldstone ones by integration over frequencies.

Inserting (111) into the direct term (113), we get

$$\Sigma_d^{(2)} = i \iint d^3r_i d^3r_j \int \frac{d\omega}{2\pi} \hat{G}_{12}(\varepsilon + \omega) \hat{Q}_{1i} \hat{Q}_{j2} \times \sum_a \left(|a\rangle_2 \langle a|_1 \hat{G}_{12}^{\text{ex}}(\varepsilon_a - \omega) + |a\rangle_1 \langle a|_2 \hat{G}_{21}^{\text{ex}}(\varepsilon_a + \omega) \right). \quad (115)$$

The two required frequency integrals:

$$\begin{aligned} \int \frac{d\omega}{2\pi} \hat{G}_{12}(\varepsilon + \omega) \hat{G}_{ij}^{\text{ex}}(\varepsilon_a - \omega) &= -i \sum_{nm} \frac{|n\rangle_1 \langle n|_2 |m\rangle_i \langle m|_j}{\varepsilon + \varepsilon_a - \varepsilon_m - \varepsilon_n}, \\ \int \frac{d\omega}{2\pi} \hat{G}_{12}(\varepsilon + \omega) \hat{G}_{ji}^{\text{ex}}(\varepsilon_a + \omega) &= -i \sum_{bn} \frac{|b\rangle_1 \langle b|_2 |n\rangle_j \langle n|_i}{\varepsilon - \varepsilon_a - \varepsilon_b + \varepsilon_n}, \end{aligned} \quad (116)$$

are evaluated using Eqs. (107) and (106), respectively, noting that only the excited states appear in the expansion for G^{ex} . Bringing these together, and evaluating the direct matrix element (using notation $|ab\rangle_{12} = |a\rangle_1 |b\rangle_2$), we have:

$$\begin{aligned} \delta\varepsilon_v^d &= \langle v | \Sigma_d^{(2)} | v \rangle \\ &= \sum_{anm} \frac{\langle va | Q | nm \rangle \langle mn | Q | av \rangle}{\varepsilon + \varepsilon_a - \varepsilon_m - \varepsilon_n} + \sum_{abn} \frac{\langle vn | Q | ba \rangle \langle ab | Q | nv \rangle}{\varepsilon - \varepsilon_a - \varepsilon_b + \varepsilon_n} \\ &= \sum_{anm} \frac{g_{vanm} g_{mnv}}{\varepsilon + \varepsilon_a - \varepsilon_m - \varepsilon_n} + \sum_{abn} \frac{g_{vnba} g_{abnv}}{\varepsilon - \varepsilon_a - \varepsilon_b + \varepsilon_n}, \end{aligned} \quad (117)$$

which is the expression from Goldstone diagrams (a) and (c).

For the exchange term, we first integrate over ω_1 , with:

$$\begin{aligned} & \int \frac{d\omega_1}{2\pi} \hat{G}_{1i}(\varepsilon + \omega_1) \hat{G}_{ij}(\varepsilon + \omega_1 + \omega_2) \\ &= i \sum_{an} \left(\frac{|a\rangle_1 \langle a|_i |n\rangle_i \langle n|_j}{\omega_2 + \varepsilon_a - \varepsilon_n} + \frac{|n\rangle_1 \langle n|_i |a\rangle_i \langle a|_j}{-\omega_2 + \varepsilon_a - \varepsilon_n} \right) \\ &= i \sum_a \left[|a\rangle_1 \langle a|_i \hat{G}_{ij}^{\text{ex}}(\varepsilon_a + \omega_2) + \hat{G}_{1i}^{\text{ex}}(\varepsilon_a - \omega_2) |a\rangle_i \langle a|_j \right] \quad (118) \\ &\equiv i \hat{\Gamma}_{1ij}(\omega_2) \quad (119) \end{aligned}$$

which was evaluated using Eq. (106). The Γ_{1ij} term is defined for notational brevity; note the similarity+difference to Π_{ij} . This leads to two separate integrals over ω_2 :

$$\begin{aligned} & \int \frac{d\omega_2}{2\pi} \hat{G}_{ij}^{\text{ex}}(\varepsilon_a + \omega_2) \hat{G}_{j2}(\varepsilon + \omega_2) = i \sum_{bn} \frac{|n\rangle_i \langle n|_j |b\rangle_j \langle b|_2}{\varepsilon_a - \varepsilon + \varepsilon_b - \varepsilon_n}, \\ & \int \frac{d\omega_2}{2\pi} \hat{G}_{1i}^{\text{ex}}(\varepsilon_a - \omega_2) \hat{G}_{j2}(\varepsilon + \omega_2) = i \sum_{nm} \frac{|m\rangle_1 \langle m|_i |n\rangle_j \langle n|_2}{\varepsilon_m + \varepsilon_n - \varepsilon - \varepsilon_a}, \quad (120) \end{aligned}$$

which were evaluated using Eqs. (106) and (107), respectively. Finally, combining all the terms, we have:

$$\begin{aligned} \delta\varepsilon_v^x &= \langle v | \Sigma_x^{(2)} | v \rangle \\ &= - \sum_{abn} \frac{\langle vn | Q | ab \rangle \langle ab | Q | vn \rangle}{\varepsilon - \varepsilon_a - \varepsilon_b + \varepsilon_n} - \sum_{anm} \frac{\langle va | Q | mn \rangle \langle mn | Q | av \rangle}{\varepsilon + \varepsilon_a - \varepsilon_m - \varepsilon_n} \\ &= - \sum_{anm} \frac{g_{vnab} g_{abvn}}{\varepsilon - \varepsilon_a - \varepsilon_b + \varepsilon_n} - \sum_{abn} \frac{g_{vman} g_{mnva}}{\varepsilon + \varepsilon_a - \varepsilon_m - \varepsilon_n}, \quad (121) \end{aligned}$$

which is exactly the expression from Goldstone diagrams (d) and (b), respectively (note that $g_{ijkl} = g_{jilk}$).

7.5 Angular separation

Using the same angular identities used for the Goldstone case:

$$\sum_{m_{i,j,k,l}} g_{ijkl} g_{lkji} = \sum_{\mu} \frac{1}{[\mu]} \left(C_{ik}^{\mu} C_{jl}^{\mu} R_{ijkl}^{\mu} \right)^2 \quad (122)$$

$$\begin{aligned} \sum_{m_{i,j,k,l}} g_{ijkl} g_{klji} &= \sum_{\mu\lambda} (-1)^{\mu+\lambda+1} C_{ik}^{\mu} C_{jl}^{\mu} C_{il}^{\lambda} C_{jk}^{\lambda} \\ &\quad \times \left\{ \begin{matrix} j_i & j_k & \mu \\ j_j & j_l & \lambda \end{matrix} \right\} R_{ijkl}^{\mu} R_{ijlk}^{\lambda} \quad (123) \end{aligned}$$

$$= \sum_{\mu\lambda} (-1)^{\mu+\lambda+1} L_{ijkl}^{\mu\lambda} R_{ijkl}^{\mu} R_{ijlk}^{\lambda}, \quad (124)$$

where $L_{ijkl}^{\mu\lambda}$ is defined for convenience in the last line, the correlation potential (for angular state κ_v) can be written:

$$\Sigma_{12,d}^{(\kappa_v)} = \int \frac{d\omega}{2\pi} \sum_k \sum_{\alpha} \frac{(C_{v\alpha}^k)^2}{[j_v]} g_{12}^{\alpha}(\varepsilon + \omega) \sum_{ij} \hat{q}_{1i}^k \hat{\pi}_{ij}^k(\omega) \hat{q}_{j2}^k, \quad (125)$$

$$\begin{aligned} \Sigma_{12,x}^{(\kappa_v)} &= \iint \frac{d\omega_1}{2\pi} \frac{d\omega_2}{2\pi} \sum_{k\lambda} \frac{(-1)^{k+\lambda}}{[j_v]} \sum_{\alpha,\beta,\gamma} L_{v\beta\alpha\gamma}^{k\lambda} \\ &\quad \times \sum_{ij} g_{1i}^{\alpha}(\varepsilon + \omega_1) \hat{q}_{1j}^{\alpha} g_{ij}^{\beta}(\varepsilon + \omega_1 + \omega_2) \hat{q}_{i2}^{\lambda} g_{j2}^{\gamma}(\varepsilon + \omega_2). \quad (126) \end{aligned}$$

Here, the k and λ sums are over Coulomb multipolarities, and the $(\kappa = \alpha, \beta, \gamma)$ sum is over angular quantum numbers (partial waves). In theory, the k and κ sums are infinite; in practice one (or both) must be truncated. The ij sum is the finite-grid

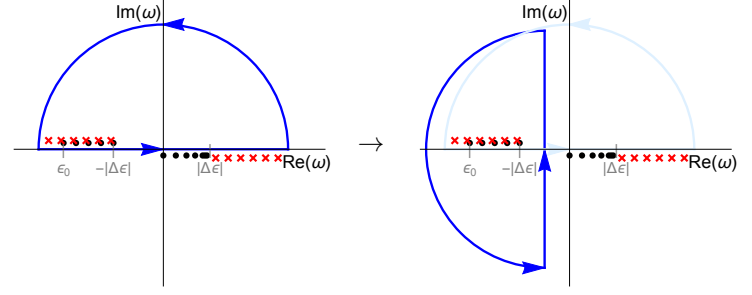


Figure 8: Rotation of the contour for integrals in the form of Eq. (131). Dots represent Green's function poles, crosses are polarisation operator poles (only bound-state poles are shown, there are also continuum-state poles at larger $|\omega|$), ε_0 is the energy of the deepest core state, and $|\Delta\varepsilon|$ is the energy gap between the core and excited bound states.

implementation of radial integrals; the integration measures are included in q_{ij} .

The radial Green's function is

$$g_{12}^{\alpha}(\varepsilon) = \sum_n^{\kappa_{\alpha}} \frac{F_{n\alpha}(r_1) F_{n\alpha}^{\dagger}(r_2)}{\varepsilon - \varepsilon_{n\alpha}} = \frac{\chi_0^{\alpha}(r_{<}) \chi_{\infty}^{\alpha}(r_{>})}{w}, \quad (127)$$

where the sum runs over all orbitals with $\kappa = \kappa_{\alpha}$, and the χ are solutions to the radial Dirac equation with $\kappa = \kappa_{\alpha}$. As described above, g should be corrected to account for exchange, with

$$V_{x,12}^{(\kappa_v)} = \frac{-1}{[j_v]} \sum_a^{\text{core}} \sum_{\lambda} (C_{av}^{\lambda})^2 F_a(r_1) F_a^{\dagger}(r_2) \hat{q}_{12}^{\lambda}. \quad (128)$$

The radial Coulomb operator is (see Laplace expansion)

$$\hat{q}_{ij}^k = \frac{r_{<}^k}{r_{>^{k+1}}} dr_i dr_j, \quad (129)$$

and the radial polarisation operator is

$$\pi_{12}^k(\omega) = i \sum_a^{\text{core}} p_{12}^a \sum_n^{(\kappa)} \frac{(C_{an}^k)^2}{[k]} \left[g_{12}^{\text{ex},n}(\varepsilon_a - \omega) + g_{12}^{\text{ex},n}(\varepsilon_a + \omega) \right], \quad (130)$$

where

$$p_{ij}^a = F_a(r_i) F_a^{\dagger}(r_j)$$

is the (radial) projection operator onto single core state a .

7.6 Numerical frequency integration

The direct and exchange potentials involve integrals of the form:

$$\int g(\varepsilon + w) \pi(\omega) \dots \frac{d\omega}{2\pi}. \quad (131)$$

The integrand contains poles from the Green's function at $\omega = \varepsilon_n - \varepsilon - i\delta$ and $\omega = \varepsilon_a - \varepsilon + i\delta$, and poles from the polarisation operator at $\omega = \varepsilon_a - \varepsilon_n + i\delta$ and $\omega = \varepsilon_n - \varepsilon_a - i\delta$. If ε is the energy of the lowest excited state, then there are an infinite number of poles from the polarisation operator in each of the regions $\omega < -|\Delta\varepsilon|$, and $|\Delta\varepsilon| < \omega < \infty$, where $\Delta\varepsilon$ is the energy gap between the highest core and lowest excited states (for Cs, $|\Delta\varepsilon| \approx 0.7$ au). From the Green's function, there are a finite number (equal to the number of core states) of poles in the region $-|\varepsilon_0| < \omega < -|\Delta\varepsilon|$, and an infinite number of poles in the region $\omega > 0$ (see Fig. 8).

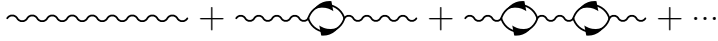


Figure 9: Screening of the Coulomb interaction: each Coulomb line is replaced with this infinite series of screening diagrams.

If we were to evaluate the integral (131) numerically using a semi-circle contour closed in the upper/lower-half of the complex plane, it would involve evaluating the integrand arbitrarily close to the poles, which is problematic. Instead, we rotate the integration contour anti-clockwise by 90° ; the straight part of the contour is at fixed $\text{Re}(\omega)$. This is shown in Fig. 8. It is clear from Cauchy's theorem that the integral over each of the contours is the same and equal to the required integral (131).

Using the contour as shown in Fig. 8, the integral becomes

$$\int_{-\infty}^{\infty} g(\varepsilon + \omega_r + i\omega_i) \pi(\omega_r + i\omega_i) \dots \frac{d\omega_i}{2\pi} + \oint_{\text{curved}} \dots \quad (132)$$

If the contour radius (i.e., maximum value of ω_i) is large enough, the value of the integrand around the curved part of the contour ≈ 0 , so only the ω_i integral needs to be evaluated. It is desirable to place ω_r , which remains constant throughout the integration, as far away from the poles as possible. There is a region with no poles between 0 and $|\Delta\varepsilon|$, so we take $\omega_r \simeq -|\Delta\varepsilon|/2$.

Finally, to perform the integrals numerically, we must evaluate Green's functions at complex frequency values: $\omega = \omega_r + i\omega_i$. This can be done in analogy with Eq. (100):

$$g(\varepsilon + \omega) = [1 + i\omega_i g(\varepsilon + \omega_r)]^{-1} g(\varepsilon + \omega_r) \quad (133)$$

This $g(\varepsilon + \omega)$ will be a complex-valued matrix; $g(\varepsilon + \omega_r)$ is real-valued. The integration over ω_i can then proceed using standard numerical integration.

8 All-orders correlation potential

The three most important corrections beyond the second-order correlation potential are: (i) the screening of the residual Coulomb interaction by the core electrons [24], (ii) the hole-particle interaction [26], and (iii) the chaining of the Σ operator [22, 23]. These effects are described by a series of diagrams that can be summed exactly to all-orders using the Feynman technique. The method described here was developed in the above works, and may be called the *Dzuba-Flambaum-Sushkov* (DFS) method; it is also called the *perturbation theory in the screened Coulomb interaction* (PTSCI) method.

It is important to stress a key advantage of the current method: its numerical efficiency. Using the Feynman approach for the second-order (direct) diagrams takes roughly the same computational power as using the Goldstone method (in fact, it is a bit faster). Then, the inclusion of the all-orders screening and hole-particle interaction has effectively *no* impact on the computer time required. That is, calculating the all-orders correlation potential is roughly just as computationally intensive as calculating the second-order corrections using the usual (Goldstone) many-body approach. This is in stark contrast to other methods (e.g., coupled-cluster), which require *huge* computational resources for all-orders calculations. Further, our method takes into account screening effects with double, triple, quadruple, and higher core excitations, in contrast to all-order coupled-cluster methods, which typically include only double (and sometimes partial triple) excitations.



Figure 10: Hole-particle corrections to the polarisation operator

8.1 Screening of the residual Coulomb interaction

The most important correction is the screening of the residual Coulomb interaction by the core electrons, which can be taken into account by a continued insertion of polarisation loops into the Coulomb lines, as shown in Fig. 9. This chain of diagrams represent the matrix geometric series:

$$\tilde{Q} \equiv \hat{Q} + \hat{Q}(-i\hat{\Pi}\hat{Q}) + \hat{Q}(-i\hat{\Pi}\hat{Q})^2 + \dots \quad (134)$$

Note that each additional $\hat{\Pi}\hat{Q}$ term carries a factor of $(-i)$ due to Eq. (109). The series may be summed exactly as

$$\tilde{Q}(\omega) = \hat{Q} [1 + i\hat{\Pi}(\omega)\hat{Q}]^{-1} = [1 + i\hat{Q}\hat{\Pi}(\omega)]^{-1} \hat{Q}. \quad (135)$$

This is the screened Coulomb operator, and includes electron screening to all-orders. This is enhanced by the number of electrons in the outermost core shell, and the relatively small energy denominator associated with their excitation, see Eq. (111). We could also instead write the series (134) as $\hat{Q}\tilde{\Pi}\hat{Q}$, with

$$\tilde{\Pi}(\omega) = \hat{\Pi}(\omega) [1 + i\hat{Q}\hat{\Pi}(\omega)]^{-1} = [1 + i\hat{\Pi}(\omega)\hat{Q}]^{-1} \hat{\Pi}(\omega). \quad (136)$$

Inserting the screened Coulomb operator into Eqs. (113) and (114) yields the new correlation potential:

$$\Sigma_d = \iint d^3r_i d^3r_j \int \frac{d\omega}{2\pi} \hat{G}_{12}(\varepsilon + \omega) \hat{Q}_{1i} \hat{\Pi}_{ij}(\omega) \tilde{Q}_{j2}(\omega), \quad (137)$$

$$\Sigma_x = - \iint d^3r_i d^3r_j \iint \frac{d\omega_1}{2\pi} \frac{d\omega_2}{2\pi} \times \hat{G}_{1i}(\varepsilon + \omega_1) \tilde{Q}_{1j}(\omega_1) \hat{G}_{ij}(\varepsilon + \omega_1 + \omega_2) \tilde{Q}_{j2}(\omega_2) \hat{G}_{j2}(\varepsilon + \omega_2), \quad (138)$$

which includes screening to all-orders. Note that the screened operator should replace only a single Coulomb line in the direct diagram, but both in the exchange diagram.

Note that this method takes into account screening diagrams with double, triple, quadruple, and higher core electron excitations. This is because the Feynman diagram technique contains all possible time orderings of the polarisation loops; therefore the screening diagrams contain any number of excited electrons [24]. This is in contrast to the widely-used “singles-doubles coupled-cluster method”, where only double excitations are considered (and sometimes a selection of important triple excitations). There are, however, some perturbation-theory diagrams included in the coupled-cluster methods that are not included in our approach. The most important of which (the so-called ladder diagrams) are very small, and can be included into our method by means of the method presented in Ref. [28].

8.2 Hole-particle interaction

The chain of diagrams corresponding to the hole-particle interaction is shown in Fig. 10. Physically, this effect arises due to the deviation of the (direct) Hartree-Fock potential for the excited core electron in the polarisation loop from that for the non-excited one [26]. In other words, it corresponds to an alteration of the core potential due to the excitation of the particle

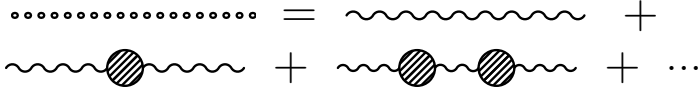


Figure 11: All-order screening of the Coulomb operator including the hole-particle interaction.

from the core to the virtual intermediate state; the excited core particle in the polarisation loop moves in the field of $N-2$ other core electrons instead of the usual V^{N-1} potential.

In practical Hartree-Fock calculations for occupied core states, the self-interaction term is included in the direct potential; this is then exactly compensated by the corresponding term in the exchange potential. However, for the state excited from the core ($a_n^\dagger a_a |0\rangle$), no such cancellation occurs. Therefore, the self-interaction term should be removed for the excited states.

Following the approach from Ref. [26], the potential that simultaneously describes the occupied core and excited states is

$$\hat{V} = V^{N-1} - (1 - \hat{P}_{\text{core}})V_0(1 - \hat{P}_{\text{core}}), \quad (139)$$

where

$$\hat{P}_{\text{core}} = \sum_a^{\text{core}} |a\rangle\langle a| \quad (140)$$

is the operator of projection onto the core, and V_0 is the zero-multipolarity potential for the outgoing electron. We use Eq. (139) since the Green's function contains both core and excited electrons [see Eq. (96)]; \hat{P} is introduced to ensure orthogonality of the orbitals. The G^{ex} function that appears in the polarisation operator is then formed as Eq. (112). Note that $\langle V \rangle = \langle V^{N-1} \rangle$ for the occupied core states, and $\langle V \rangle = \langle V^{N-1} \rangle - \langle V_0 \rangle$ for the excited states. In this method, we do not calculate the hole-particle diagrams directly. We calculate the Green's function using the potential in Eq. (139), and use it to form the polarisation operator. This corrected polarisation operator includes the dominating hole-particle effects.

We may include the “corrected” polarisation operator in place of the regular polarisation operator when calculating the screened Coulomb line, as shown in Fig. 11. Inserting the corrected polarisation loop, and the screened Coulomb lines into the diagrams for the correlation potential, we obtain an expression for the all-order correlation potential as shown in Fig. 12.

8.3 Self-energy chaining

The “chaining” of the correlation potential (iteration of Σ) is shown in Fig. 13. This is accounted for automatically by including Σ into the Hartree-Fock iterations for the valence orbital (correlation potential method, as described previously). This is an important effect that includes terms with excitations of the external valence electron, and is enhanced due to the small energy denominator associated with this excitation. Because the Hartree-Fock equations (with Σ) are iterated until self-consistency is reached, the chaining is included to all-orders.

8.4 Effective screening for exchange term

In the all-orders method, the frequency integrations can no longer be performed analytically. This is fine for the direct potential, since it contains only a single integral (the frequency integral inside the polarisation operator can be done analytically). The exchange potential, on the other hand, contains a double integral over frequencies, which is numerically expensive.

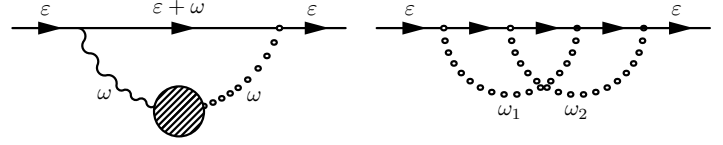


Figure 12: All-order correlation diagrams including the Coulomb screening and hole-particle interaction.

The exchange contribution to the correlation potential is typically small compared to the direct potential, and the screening is a small correction to this. Therefore, it seems reasonable to approximately account for the screening in the exchange potential. This is done by introducing effective screening factors for the Coulomb operator in the exchange potential: $\hat{Q} \approx f\hat{Q}$. In practice, the Coulomb operator is expanded over multiplicities $\hat{Q} \sim \sum_k \hat{q}^k$ (Laplace expansion, as discussed previously), and a different screening factor is used for each multiplicity:

$$\tilde{q}^k(\omega) \approx f_k \hat{q}^k. \quad (141)$$

Note that the frequency dependence of f_k has been neglected.

The screening factors are calculated by evaluating the direct energy correction (for each k) with and without screening:

$$f_k = \langle v | \Sigma_d^{(\text{screened}),k} | v \rangle / \langle v | \Sigma_d^{(2),k} | v \rangle. \quad (142)$$

Then, the frequency integrals for the exchange term can be carried out analytically, and the exchange potential may be calculated by summation over a complete set of states in exact analogy to the Goldstone case, just with the extra k -dependent factors. This greatly improves the efficiency of the exchange part of the calculation, while still maintaining good accuracy.

The hole-particle interaction is not included in Σ for calculation of f_k (hole-particle effect enters at third-order in the direct diagrams, but only at fourth-order in exchange). However, this means the hole-particle effect is not included into the exchange diagrams at all, which in certain cases may be important. The screening effect is also taken into account approximately, which may also be important in some cases.

9 Structure radiation + renormalisation: Correlation corrections to matrix elements²⁴

By using Brueckner orbitals (correlation potential method) to compute matrix elements and including core polarisation, the dominating correlation corrections to matrix elements are included automatically. However, effects that involve terms where the external field acts inside the correlation diagrams – known as structure radiation – cannot be included into the correlation potential method, and must be considered separately [20, 29]. This is illustrated in Fig. 14. In total, there are 36 such diagrams; 9 for each of the four second-order diagrams in Fig. 5. At the same level there enters another correction, known as normalisation of states, that also cannot be included into the correlation potential method. It arises due to the change of the

²⁴Implemented in: /src/MBPT/StructureRad.hpp

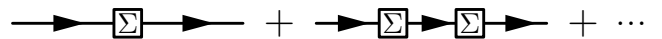


Figure 13: Chaining of the correlation potential (self-energy); the boxed Σ refers to the sum of diagrams in Fig. 12.

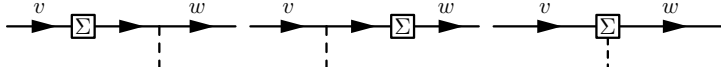


Figure 14: Correlation corrections to matrix elements: Σ represents the correlation potential, and the dashed line is interaction with external field. The first two diagrams are included when Brueckner orbitals are used to compute the matrix elements; the third diagram, called structure radiation, is not.

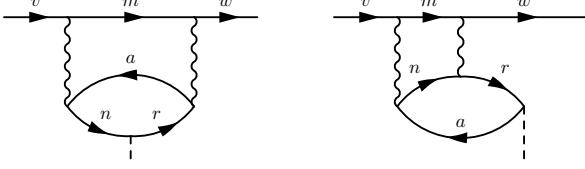


Figure 15: Example structure radiation diagrams, showing a “centre” (left) and “top” (right) diagram.

normalisation of the wavefunctions due to configuration mixing. All these effects are suppressed compared to the Brueckner and core-polarisation corrections (roughly) by the ratio of the core excitation energy to that of the valence states.

Matrix elements of operator \hat{h} (rank k) are written [20, 29]:

$$\langle w|h|v\rangle + \langle w|\delta h^{\text{SR}}|v\rangle + \langle w|\delta h^{\text{Norm}}|v\rangle. \quad (143)$$

The normalisation contributions can be expressed

$$\langle w|\delta h^{\text{Norm}}|v\rangle = \frac{-1}{2} \langle w|h|v\rangle (N_w + N_v), \quad (144)$$

where (using the short-hand $\varepsilon_{ij} \equiv \varepsilon_i + \varepsilon_j$)

$$N_v = \sum_{amn} \frac{\delta \Sigma_{vamn}}{\varepsilon_{va} - \varepsilon_{mn}} + \sum_{abn} \frac{\delta \Sigma_{vnab}}{\varepsilon_{vn} - \varepsilon_{ab}}, \quad (145)$$

with

$$\delta \Sigma_{vijk} = \sum_{\mu} \frac{1}{[\mu][j_v]} \left(\frac{Q_{vijk}^{\mu} W_{vijk}^{\mu}}{\varepsilon_{vi} - \varepsilon_{jk}} \right). \quad (146)$$

Note that $\delta \Sigma$ are just individual contributions to the second-order energy shift, Eq. (86); see Ref. [20] for discussion.

The structure radiation terms are more complicated. Following Ref. [30], they can be broken into three groups of 12 diagrams: “top” (T), “bottom” (B), and “centre” (C):

$$\langle w|\delta h^{\text{SR}}|v\rangle = \langle w|T|v\rangle + \langle w|B|v\rangle + \langle w|C|v\rangle.$$

Two examples are shown in Fig. 15. Expressions for these terms were presented in Ref. [30]:

$$\langle w|T|v\rangle = \sum_{ar} \frac{\langle a|h|r\rangle T_{wrv a}^k}{\varepsilon_n - \varepsilon_a + \omega}, \quad (147)$$

$$\langle w|B|v\rangle = \sum_{ar} \frac{\langle r|h|a\rangle B_{wavr}^k}{\varepsilon_n - \varepsilon_a - \omega}, \quad (148)$$

$$\langle w|C|v\rangle = - \sum_{ab} \langle b|h|a\rangle C_{wav b}^k - \sum_{rn} \langle r|h|n\rangle D_{wnvr}^k, \quad (149)$$

where ω is the transition frequency, a, b, c, \dots are states in the core (holes), n, m, r, \dots are virtual excited states, and w, v are valence states. For diagonal matrix elements $T = B$.

The T^k terms are written as $T = T^1 + T^2 + T^3 + T^4$, with:²⁵

$$\begin{aligned} T_{wrv c}^{1,k} &= \sum_{ab\mu\lambda} (-1)^{v+r+a+b+k} \begin{Bmatrix} w & v & k \\ \lambda & \mu & b \end{Bmatrix} \begin{Bmatrix} r & c & k \\ \lambda & \mu & a \end{Bmatrix} \frac{W_{wrb a}^{\mu} Q_{vabc}^{\lambda}}{\varepsilon_{wr} - \varepsilon_{ba}} \\ T_{wrv c}^{2,k} &= \sum_{an\mu} \frac{(-1)^{w-c+k+\mu}}{[\mu]} \begin{Bmatrix} w & v & k \\ r & c & \mu \end{Bmatrix} \frac{W_{wacn}^{\mu} W_{varn}^{\mu}}{\varepsilon_{rn} - \varepsilon_{va}} \\ T_{wrv c}^{3,k} &= \sum_{an\mu} \frac{(-1)^{w-c+k+\mu}}{[\mu]} \begin{Bmatrix} w & v & k \\ r & c & \mu \end{Bmatrix} \frac{W_{wnca}^{\mu} W_{vnra}^{\mu}}{\varepsilon_{wn} - \varepsilon_{ca}} \\ T_{wrv c}^{4,k} &= \sum_{mn\mu\lambda} (-1)^{v+r+n+m+k} \begin{Bmatrix} w & v & k \\ \lambda & \mu & n \end{Bmatrix} \begin{Bmatrix} r & c & k \\ \lambda & \mu & m \end{Bmatrix} \frac{Q_{wrnm}^{\mu} W_{vcnm}^{\lambda}}{\varepsilon_{nm} - \varepsilon_{vc}}. \end{aligned} \quad (150)$$

(T^1 and T^4 each correspond to two diagrams; T^2 and T^3 each correspond to four). The B terms are similar:

$$B_{wavr}^k = (-1)^{v-w+a-r} T_{vrwa}^k. \quad (151)$$

Finally, the centre C and D terms are:

$$\begin{aligned} C_{wav c}^k &= \sum_{bn\mu} \frac{(-1)^{k+\mu}}{[\mu]} \begin{Bmatrix} w & v & k \\ c & a & \mu \end{Bmatrix} \frac{(-1)^{w-c} W_{wnab}^{\mu} W_{vncb}^{\mu}}{(\varepsilon_{wn} - \varepsilon_{ab})(\varepsilon_{vn} - \varepsilon_{bc})} \\ &+ \sum_{mn\mu\lambda} (-1)^k \begin{Bmatrix} w & v & k \\ \mu & \lambda & n \end{Bmatrix} \begin{Bmatrix} c & a & k \\ \lambda & \mu & m \end{Bmatrix} \frac{(-1)^{v+a+m+n} Q_{vmnc}^{\mu} W_{wanm}^{\lambda}}{(\varepsilon_{wa} - \varepsilon_{nm})(\varepsilon_{vc} - \varepsilon_{nm})} \\ D_{wrv m}^k &= \sum_{an\mu} \frac{(-1)^{k+\mu}}{[\mu]} \begin{Bmatrix} w & v & k \\ m & r & \mu \end{Bmatrix} \frac{(-1)^{w-m} W_{wavn}^{\mu} W_{vamn}^{\mu}}{(\varepsilon_{wa} - \varepsilon_{rn})(\varepsilon_{va} - \varepsilon_{mn})} \\ &+ \sum_{ab\mu\lambda} (-1)^k \begin{Bmatrix} w & v & k \\ \mu & \lambda & a \end{Bmatrix} \begin{Bmatrix} m & r & k \\ \lambda & \mu & b \end{Bmatrix} \frac{(-1)^{v+r+a+b} Q_{vbam}^{\mu} W_{wrab}^{\lambda}}{(\varepsilon_{wr} - \varepsilon_{ab})(\varepsilon_{vm} - \varepsilon_{ab})}. \end{aligned} \quad (152)$$

The dominating uncertainty for these corrections comes from completeness of the basis. In particular, the structure radiation terms involve matrix elements of \hat{h} between basis states (the normalisation of states only contains matrix elements between valence states). It is therefore a good test to perform the core-polarisation calculations using both the TDHF (Sec. 5.3) and diagram (Sec. 5.4) methods using the same basis as for structure radiation, since the diagram RPA method also involves matrix elements between basis states. If the TDHF and diagram core polarisation calculations match, it is good indication that the basis is sufficient to also describe the structure radiation.

10 Relativity beyond Dirac-Coulomb (Breit+QED)

The Dirac equation as presented in Eq. (25) accounts for the relativistic motion of the electron in the Coulomb field of the nucleus, however, it treats the Coulomb field classically, and treats the electron-electron Coulomb repulsion non-relativistically (see, e.g., Ref. [1]). For high-accuracy calculations, and particularly for atoms with large Z , corrections due to the missing relativistic effects become important ($\sim 0.1 - 1\%$). The two corrections considered here are the Breit interaction, which contains the dominating relativistic corrections to the electron-electron Coulomb interaction, and the radiative quantum electrodynamics (QED) corrections, which are accounted for via the Ginges-Flambaum radiative potential method.

Our Breit corrections are compared against those calculated by Derevianko in Ref. [33]. There, it was demonstrated that the interplay between the Breit effects and correlations were crucial

²⁵Using notation $\varepsilon_{ij} \equiv \varepsilon_i + \varepsilon_j$, and e.g., ‘ a ’ short for j_a in 6j symbols and phase factors, e.g., $(-1)^{a+b} \equiv (-1)^{j_a+j_b}$, while k, μ, λ are multipolarities.

Table 7: Breit and QED corrections to the removal energies of the lowest s and p states of Cs, as calculated at the Hartree-Fock and $\Sigma^{(2)}$ levels (units: cm^{-1}). First column (ε) shows energy without QED or Breit. The Breit corrections at the HF level agree exactly with Derevianko [33].

ε ($\Sigma^{(2)}$)	δQED		δBreit			Ref. [33]
	HF	$\Sigma^{(2)}$	HF	$\Sigma^{(2)}$		
$6s_{1/2}$	32412.1	-16.0	-23.7	-3.2	2.9	2.6
$7s_{1/2}$	13023.0	-4.3	-5.2	-1.1	-0.1	0.3
$6p_{1/2}$	20537.8	0.8	1.1	-7.5	-7.3	-7.1
$7p_{1/2}$	9710.0	0.3	0.4	-2.7	-2.6	-2.5
$6p_{3/2}$	19939.2	0.1	0.0	-2.9	-0.6	-0.8
$7p_{3/2}$	9520.5	0.0	0.0	-1.0	-0.4	-0.4

Table 8: QED corrections to the electric dipole (E1) reduced matrix elements of lowest s and p states of Cs at the HF, RPA, and $\Sigma^{(2)}$ levels (units: a_B). First column shows E1 (absolute value) at the RPA+ $\Sigma^{(2)}$ level, without QED (or Breit).

	E1	δ QED		
		HF	RPA	RPA+ $\Sigma^{(2)}$
$6p_{1/2}-6s_{1/2}$	4.3874	0.0033	0.0033	0.0035
$7p_{1/2}-6s_{1/2}$	0.3001	-0.0025	-0.0024	-0.0023
$6p_{3/2}-6s_{1/2}$	6.1698	0.0048	0.0049	0.0052
$7p_{3/2}-6s_{1/2}$	0.6056	-0.0029	-0.0028	-0.0025
$7p_{1/2}-7s_{1/2}$	10.178	0.0069	0.0069	0.0072
$7p_{3/2}-7s_{1/2}$	14.123	0.0099	0.0099	0.0103
$7s_{1/2}-6p_{1/2}$	4.2241	-0.0046	-0.0044	-0.0045
$7s_{1/2}-6p_{3/2}$	6.4705	-0.0058	-0.0056	-0.0054

– even changing the sign of the Breit contribution in many cases. Our Breit calculations agree perfectly with those of Ref. [33] at the HF level, and agree very well including correlations. The interplay between the QED and correlation corrections turns out also to be important [35, 36], so for high-accuracy calculations, the Breit and QED effects must be included together including correlations.

Tables 7, 8, and 9 show the QED and Breit corrections to the lowest s and p energies and E1 matrix elements at various levels of approximation. The combination of correlation corrections with the Breit and QED effects are important.

10.1 Breit interaction²⁶

This section mostly follows Ref. [3]; see also [31–33]. The Breit Hamiltonian accounts for magnetic interactions between electrons (also known as the Gaunt interaction), and retardation

²⁶Implemented in: /src/HF/Breit.hpp

Table 9: Breit corrections to the E1 reduced matrix elements of s and p states of Cs at the HF, RPA, and $\Sigma^{(2)}$ levels (units: a_B). Corrections at the HF level agree near-perfectly with Derevianko [33].

	E1	δ Breit			
		HF	RPA	RPA+ $\Sigma^{(2)}$	Ref. [33]
$6p_{1/2}-6s_{1/2}$	4.387	0.0004	0.0000	-0.0008	-0.0010
$7p_{1/2}-6s_{1/2}$	0.300	0.0018	0.0016	0.0017	0.0019
$6p_{3/2}-6s_{1/2}$	6.170	0.0008	0.0001	-0.0009	-0.0011
$7p_{3/2}-6s_{1/2}$	0.606	0.0006	0.0003	0.0002	0.0005
$7p_{1/2}-7s_{1/2}$	10.178	-0.0010	-0.0011	-0.0022	-0.0029
$7p_{3/2}-7s_{1/2}$	14.123	0.0008	0.0006	0.0004	-0.0013
$7s_{1/2}-6p_{1/2}$	4.224	0.0046	0.0045	0.0045	0.0049
$7s_{1/2}-6p_{3/2}$	6.471	0.0018	0.0018	0.0010	0.0016

effects (see, e.g., [1]). It leads to a correction to the electron-electron Coulomb term in the many-body Hamiltonian (25):

$$\sum_{ij} \frac{1}{r_{ij}} \rightarrow \sum_{ij} \left(\frac{1}{r_{ij}} + \hat{h}_{ij}^B \right), \quad (153)$$

where, in the limit of zero frequency, the two-particle Breit Hamiltonian is

$$\hat{h}_{ij}^B = -\frac{\boldsymbol{\alpha}_i \cdot \boldsymbol{\alpha}_j + (\boldsymbol{\alpha}_i \cdot \hat{\mathbf{n}}_{ij})(\boldsymbol{\alpha}_j \cdot \hat{\mathbf{n}}_{ij})}{2r_{ij}}. \quad (154)$$

Frequency-dependent effects can be neglected in most situations, see, e.g., discussion in Refs. [1, 3].

Inclusion of the Breit Hamiltonian into the Hartree-Fock equations [33] leads to a correction to the HF potential (28):

$$\hat{V}_{\text{HF}} \rightarrow \hat{V}_{\text{HF}} + \hat{V}_{\text{Br}}. \quad (155)$$

Inclusion into the Hartree-Fock and TDHF equations allows for the inclusion of Breit effects into the calculations of atomic energies and wavefunctions. Since the Breit potential depends on the core orbitals, an extra term now also appears in the TDHF equations:

$$\delta V \rightarrow \delta V_{\text{HF}}(\delta\phi) + \delta V_{\text{Br}}(\delta\phi), \quad (156)$$

which in fact gives the dominant Breit correction to matrix elements in many cases.

After integration over angular coordinates, and summation over magnetic quantum numbers, the (non-local) radial Breit operator can be expressed via

$$\hat{V}_{\text{Br}} F_a(r) = \sum_b^{\text{core}} \sum_k \hat{B}_{ba}^k F_b(r), \quad (157)$$

with

$$\hat{B}_{ba}^k = \frac{(C_{ba}^k)^2}{[j_a]} \left[\hat{M}_{ba}^k + \hat{O}_{ba}^k + \hat{P}_{ba}^k \right] + \frac{(C_{-b,a}^k)^2}{[j_a]} \hat{N}_{ba}^k. \quad (158)$$

where M, N are due to the magnetic effects, O, P are due to retardation, and $C_{-b,a}^k \equiv \langle -\kappa_b || C^k || \kappa_a \rangle$. The equation for $\delta V_{\text{Br}}(\delta\phi)$ is not given explicitly here, but can be found by making the substitution in Eq. (72):

$$C_{ba}^k y_{ba}^k \rightarrow -C_{ba}^k (M_{ba}^k + O_{ba}^k + P_{ba}^k) - C_{-b,a}^k N_{ba}^k.$$

Note that while no direct Breit term appears in the HF equations, it does enter into δV_{Br} .

The magnetic terms can be expressed as

$$\begin{aligned} \hat{M}_{ba}^k &= \frac{k+1}{2k+3} [b_{ba}^{k+1}(r) + \eta_{ba}^{k+1} g_{ba}^{k+1}(r)] (\eta_{ba}^{k+1} \hat{\theta}_x - \hat{\theta}_y) \\ &\quad - \frac{k}{2k-1} [b_{ba}^{k-1}(r) - \eta_{ba}^k g_{ba}^{k-1}(r)] (\eta_{ba}^{k+1} \hat{\theta}_x + \hat{\theta}_y) \end{aligned} \quad (159)$$

and

$$\hat{N}_{ba}^k(r) = \frac{(\kappa_b + \kappa_a)^2}{k(k+1)} g_{ba}^k(r) \hat{\theta}_x, \quad (160)$$

and the retardation terms can be expressed as

$$\begin{aligned} \hat{O}_{ba}^k(r) &= \frac{(k+1)^2}{[k](2k+3)} [b_{ba}^{k+1}(r) + \eta_{ba}^{k+1} g_{ba}^{k+1}(r)] (-\eta_{ba}^{k+1} \hat{\theta}_x + \hat{\theta}_y) \\ &\quad + \frac{k^2}{[k](2k-1)} [b_{ba}^{k-1}(r) - \eta_{ba}^k g_{ba}^{k-1}(r)] (\eta_{ba}^{k+1} \hat{\theta}_x + \hat{\theta}_y), \end{aligned} \quad (161)$$

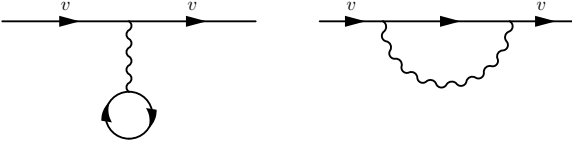


Figure 16: Vacuum polarisation (left) and self-energy (right) diagrams. In the radiative potential method, the self-energy diagram is replaced with an effective local potential [34].

and

$$\hat{P}_{ba}^k(r) = \frac{k(k+1)}{2[k]} \left[P_1(r) \left(\eta_{ba}^{k+1} \hat{\theta}_x - \hat{\theta}_y \right) - P_2(r) \left(\eta_{ba}^k \hat{\theta}_x + \hat{\theta}_y \right) \right] \quad (162)$$

with

$$P_1(r) = \left[b_{0,ba}^{k-1}(r) - \eta_{ba}^k g_{0,ba}^{k-1}(r) - b_{0,ba}^{k+1}(r) + \eta_{ba}^k g_{0,ba}^{k+1}(r) \right]$$

$$P_2(r) = \left[b_{\infty,ba}^{k-1}(r) + \eta_{ba}^{k+1} g_{\infty,ba}^{k-1}(r) - b_{\infty,ba}^{k+1}(r) - \eta_{ba}^{k+1} g_{\infty,ba}^{k+1}(r) \right].$$

In the above,

$$\hat{\theta}_x = \begin{pmatrix} 0 & 1 \\ 1 & 0 \end{pmatrix}, \quad \hat{\theta}_y = \begin{pmatrix} 0 & 1 \\ -1 & 0 \end{pmatrix} \quad (163)$$

(note: $\hat{\theta}_x = \hat{\sigma}_x$, and $\hat{\theta}_y = i\hat{\sigma}_y$, except these act in the radial spinor space only),

$$\eta_{ba}^k \equiv (\kappa_b - \kappa_a)/k, \quad (164)$$

$$b_{ij}^k(r) = \int_0^r \frac{x^k}{r^{k+1}} [f_i g_j - g_i f_j](x) dx$$

$$+ \int_r^\infty \frac{r^k}{x^{k+1}} [f_i g_j - g_i f_j](x) dx, \quad (165)$$

(with b_0/b_∞ being just the first/second term), and

$$g_{ij}^k(r) = \int_0^r \frac{x^k}{r^{k+1}} [f_i g_j + g_i f_j](x) dx$$

$$+ \int_r^\infty \frac{r^k}{x^{k+1}} [f_i g_j + g_i f_j](x) dx. \quad (166)$$

10.2 Radiative QED corrections²⁷

Radiative QED corrections can be included into the wavefunctions using the radiative potential method developed in Ref. [34], including the (small) finite nuclear size corrections [35, 36]. In this method, an effective potential, V_{rad} , is added to the Hamiltonian before the equations are solved. The potential can be written as the sum of the Uehling (vacuum polarisation) and self-energy potentials, see Fig. 16. The self-energy potential itself is written as the sum of the high- and low-frequency electric contributions, and the magnetic contribution:

$$V_{\text{rad}}(\mathbf{r}) = V_{\text{Ueh}}(r) + V_{\text{SE}}^h(r) + V_{\text{SE}}^l(r) + V_{\text{SE}}^{\text{mag}}(\mathbf{r}). \quad (167)$$

Including this potential into the Hartree-Fock equations (instead of adding it as a subsequent perturbation) gives an important contribution (core relaxation), especially for states with $l > 0$. The first three (electric) terms on the RHS of Eq. (167),

$$V^{\text{el}}(r) = V_{\text{Ueh}}(r) + V_{\text{SE}}^h(r) + V_{\text{SE}}^l(r), \quad (168)$$

are simple scalar terms, and can be included into the calculations simply (e.g., by adding them to the nuclear potential). The final (magnetic) term, which can be expressed as [36]

$$V_{\text{SE}}^{\text{mag}}(\mathbf{r}) = i(\boldsymbol{\gamma} \cdot \mathbf{n}) H^{\text{mag}}(r), \quad (169)$$

leads to off-diagonal terms in the Hamiltonian. Together, they can be included via additions to the radial derivative (12):

$$\partial_r F = \frac{1}{c} \begin{pmatrix} (-c\kappa/r + H^{\text{mag}}) & (\varepsilon - \hat{V} + V^{\text{el}} + 2c^2) \\ -(\varepsilon - \hat{V} + V^{\text{el}}) & (c\kappa/r - H^{\text{mag}}) \end{pmatrix} F. \quad (170)$$

The sign convention here for V_{rad} (i.e., with $\hat{H} \rightarrow \hat{H} - V_{\text{rad}}$) is from Ref. [34].

Detailed expressions for the individual contributions to V_{rad} are given in Refs. [34–36]²⁸ – they involve some rather nasty integrals that must be evaluated carefully. For the Uehling potential (with $\rho = r/\lambda_c$ and $\rho_n = r_N/\lambda_c$)²⁹ we have:

$$V_{\text{Ueh}}(r) = \frac{Z\alpha}{3\pi r} \int_1^\infty dt \frac{\sqrt{t^2 - 1}}{t^4} (2t^2 + 1) e^{-2t\rho} G_{\text{Ueh}}(r, t), \quad (171)$$

where r_N is the nuclear radius ($r_N = \sqrt{5/3} r_{\text{rms}}$) and

$$G_{\text{Ueh}}(r, t) = \begin{cases} 3(2t\rho_n)^{-3} [(2t\rho_n) \cosh(2t\rho_n) - \sinh(2t\rho_n)] & r \geq r_n \\ 3(2t\rho_n)^{-3} e^{2t\rho} [2t\rho - e^{-2t\rho_n} (1 + 2t\rho_n) \sinh(2t\rho)] & r < r_n. \end{cases} \quad (172)$$

Note that $G_{\text{Ueh}} \rightarrow 1$ as $r_N \rightarrow 0$.

For the electric self-energy potential, we have

$$V_{\text{SE}}^l(r) = -B_l(Z) Z^4 \alpha^3 F_{\text{SE}}^l(r) \quad (173)$$

where, with $\xi(x) \equiv (x+1)e^{-x}$,

$$F_{\text{SE}}^l(r) = \frac{3}{2rr_N^3 Z^2} \int_0^{r_N} r' [\xi(Z|r-r'|) - \xi(Z(r+r'))] dr'. \quad (174)$$

Note that $F_{\text{SE}}^l(r) = e^{-Zr/a_B}$ as $r_N \rightarrow 0$. And:

$$V_{\text{SE}}^h(r) = -A_l(Z) \frac{Z\alpha}{\pi r} \int_1^\infty dt I_1(t, Z) \times [e^{-2t\rho} G_{\text{Ueh}}(r, t) - I_2(r, t, Z)], \quad (175)$$

where G_{Ueh} is the same as from the Uehling potential,

$$I_1(r, t, Z) = \frac{1}{\sqrt{t^2 - 1}} \left\{ \frac{1}{t^2} - \frac{3}{2} + \left(1 - \frac{1}{2t^2} \right) \left[\ln(t^2 - 1) + 4 \ln \left((Z\alpha)^{-1} + \frac{1}{2} \right) \right] \right\}, \quad (176)$$

and

$$I_2(r, t, Z) = \frac{3r_A}{2r_N^3} \int_0^{r_N} r' \left[E_1(|r-r'| + r_A) 2t/\lambda_c - E_1([r+r'+r_A] 2t/\lambda_c) \right] dr', \quad (177)$$

²⁸Note: there is a small typo in Eq. (14) of Ref. [36] ($V_{\text{high}}^{\text{step}}$); the $r \leq r_N$ and $r > r_N$ terms should be swapped.

²⁹ λ_c is electron (reduced) Compton wavelength. Atomic units: $\lambda_c = \alpha$.

²⁷Functions defined in: /src/Physics/RadiativePotential.hpp

E_1 is the exponential integral, and $r_A \equiv 0.07Z^2\alpha^3$. Here, A_l and B_l are order-1 fitting factors, taken from Ref. [36]. Note that $I_2 \rightarrow e^{-2t\rho}r_A/[r/a_B + r_A]$ as $r_N \rightarrow 0$.

Finally for the magnetic form factor:

$$H^{\text{mag}}(r) = \frac{Z\alpha^2}{4\pi r^2} \int_1^\infty dt \frac{1}{t^2 \sqrt{t^2 - 1}} \times [(1 + 2t\eta)e^{-2t\rho}G_{\text{mag}}(r, t) - (\chi/\rho_n)^3], \quad (178)$$

where $\eta = \max(\rho, \rho_n)$, $\chi = \min(\rho, \rho_n)$, and

$$G_{\text{mag}} = \frac{3}{(2t\rho_n)^3} \left(e^{2t(\rho-\eta)} [2t\chi \cosh(2t\chi) - \sinh(2t\chi)] \right). \quad (179)$$

Note that $G_{\text{mag}} \rightarrow 1$ as $R_n \rightarrow 0$.

11 Demonstration for Cs

As a demonstration of the full method, I present calculations for the lowest-lying states of Cs, showing the break-down of all important contributions, and comparison with available experimental data. Calculations of the removal energies, electric dipole matrix elements, radiative lifetimes, and scalar polarisabilities are presented in tables 10, 11, 12, and 13, respectively.

The agreement with experiment is extremely good; deviations are smaller than a fraction of a percent for most s and p states. It is particularly worth noting that the radiative QED effects are *several times* larger than the deviation from experiment for the E1 transitions involving the $6s_{1/2}$ state – meaning we are really observing loop-level QED effects in atomic spectroscopy! The accuracy for d states is reasonable ($\sim 1\%$), but not at the same level as for the s and p states; for d states, missed correlation effects (e.g., ladder diagrams [28]) become important.

Note that, despite being reported separately in the tables, each individual contribution (e.g., screening, Breit QED etc.) is not calculated independently. In the tables, each subsequent column presents the change in the calculation from including the stated effect, beyond the inclusion of all prior effects; e.g., the δ h-p column in Table 10 shows the effect of the hole-particle interaction beyond the all-orders Coulomb screening. Most importantly, the Breit and QED effects depend rather strongly on correlations. The “final” columns are full calculations done including all effects from the start (and not the sum of each contribution calculated separately).

Table 10: Calculated removal energies (in cm^{-1}) for the lowest few states of ^{133}Cs , showing the contributions of each important effect, and comparison with experiment. ‘ $\delta\text{Scr.}$ ’ is the all-orders screening correction (beyond second-order); ‘ $\delta\text{h-p}$ ’ is the hole-particle interaction. Each column presents the change in the calculation from including each subsequent effect (beyond the inclusion of all prior-listed effects).

State	HF	$\delta\Sigma^{(2)}$	$\delta\text{Scr.}$	$\delta\text{h-p}$	δQED	δBreit	Final	Expt. [21]	Δ^\dagger	ϵ^\ddagger
$6s_{1/2}$	27954.1	4457.6	-1662.5	700.8	-21.7	-4.5	31423.8	31406.5	17.3	0.06%
$6p_{1/2}$	18790.5	1747.3	-602.0	348.3	1.1	-11.2	20274.1	20228.2	45.9	0.2%
$6p_{3/2}$	18388.8	1550.4	-530.8	308.1	0.1	-4.3	19712.4	19674.2	38.2	0.2%
$5d_{3/2}$	14138.5	3425.5	-1114.6	693.0	5.5	20.5	17168.3	16907.2	261.1	1.5%
$5d_{5/2}$	14162.6	3241.1	-1030.8	655.9	4.8	24.0	17057.6	16809.6	248.0	1.5%
$7s_{1/2}$	12112.2	957.0	-338.1	139.1	-5.0	-1.3	12863.7	12870.9	-7.2	-0.06%
$7p_{1/2}$	9222.6	506.1	-167.1	97.1	0.4	-3.6	9655.5	9641.1	14.4	0.15%
$7p_{3/2}$	9079.2	458.1	-150.8	88.1	0.04	-1.4	9473.3	9460.1	13.2	0.14%

$^\dagger\Delta = E_{\text{Theory}} - E_{\text{Expt.}}; \quad ^\ddagger\epsilon = \Delta/E_{\text{Expt.}}$

Table 11: Calculated reduced electric dipole (E1) matrix elements $\langle f||\hat{d}||i\rangle$ ($d = -er = -|e|r$) for transitions between lowest few states of ^{133}Cs , showing the contributions of each important effect, and comparison with experiment. $\delta\Sigma^{(\infty)}$ is the all-order correlation correction; $\delta\lambda\Sigma$ is the contribution from scaling $\Sigma \rightarrow \lambda\Sigma$, where λ is chosen to reproduce the experimental energies ($\lambda \approx 1$). (Units: a_0)

f	i	HF	δRPA	$\delta\Sigma^{(\infty)}$	δQED	δBreit	δSR	δNorm	$\delta\lambda\Sigma$	Final	Expt. [†]	Δ	ϵ
$6p_{1/2}$	$6s_{1/2}$	-5.278	0.303	0.468	-0.003	0.0001	-0.044	0.051	-0.002	-4.5047	-4.5057(16)	0.0010	-0.02%
$6p_{3/2}$	$6s_{1/2}$	7.426	-0.413	-0.671	0.005	0.0001	0.059	-0.069	0.002	6.3396	6.3398(22)	-0.0002	-0.004%
$7p_{1/2}$	$6s_{1/2}$	-0.372	0.134	-0.012	0.002	-0.002	-0.022	0.003	-0.009	-0.2784	-0.2781(4)	-0.0003	0.10%
$7p_{3/2}$	$6s_{1/2}$	0.695	-0.186	0.033	-0.003	0.0005	0.030	-0.005	0.012	0.5752	0.5742(1)	0.0010	0.17%
$6p_{1/2}$	$7s_{1/2}$	4.413	0.037	-0.212	-0.004	0.006	-0.012	-0.020	0.028	4.2356	4.249(4)	-0.013	-0.32%
$6p_{3/2}$	$7s_{1/2}$	-6.671	-0.042	0.233	0.005	-0.002	0.015	0.028	-0.035	-6.4693	-6.489(5)	0.020	0.30%
$7p_{1/2}$	$7s_{1/2}$	-11.009	0.088	0.592	-0.007	0.002	-0.010	0.027	0.022	-10.2962	-10.325(5)	0.029	-0.28%
$7p_{3/2}$	$7s_{1/2}$	15.345	-0.117	-0.880	0.010	0.0003	0.013	-0.036	-0.033	14.3026	14.344(7)	-0.041	-0.29%
$6p_{1/2}$	$5d_{3/2}$	8.978	-0.340	-1.711	-0.003	-0.009	0.044	-0.073	0.111	6.9986			
$6p_{3/2}$	$5d_{3/2}$	4.062	-0.146	-0.795	-0.001	-0.005	0.019	-0.032	0.053	3.1546			
$7p_{1/2}$	$5d_{3/2}$	-4.039	-0.107	2.214	0.003	0.018	0.020	0.024	-0.152	-2.0190			
$7p_{3/2}$	$5d_{3/2}$	-1.688	-0.048	0.978	0.002	0.007	0.009	0.010	-0.066	-0.7963			
$6p_{3/2}$	$5d_{5/2}$	12.186	-0.435	-2.273	-0.003	-0.017	0.055	-0.095	0.150	9.5686			
$7p_{3/2}$	$5d_{5/2}$	-5.025	-0.141	2.787	0.004	0.024	0.024	0.030	-0.192	-2.4868			

[†]Experimental results tabulated in Ref. [37].

Table 12: Calculated lifetimes (ns) for the lowest few states of ^{133}Cs , showing the contributions of each important effect, and comparison with experiment. Note that calculated frequencies, not experimental values, are used (except for the $n = 5, 6$ states, where the λ reproduces the experimental levels). Note that the *ab initio* column uses calculated frequencies, not experimental values; since lifetimes scale as ω^3 , this is the leading source of error (the λ correction is mostly due to this).

State	HF	δRPA	$\delta\Sigma^{(\infty)}$	δQED	δBreit	$\delta\text{SR+N}$	<i>ab initio</i>	$\delta\lambda\Sigma$	Final	Expt. [†]	Other [‡]
$6p_{1/2}$	46.06	5.78	-16.92	0.16	-0.06	0.16	35.17	-0.29	34.88	34.934(94)	34.4(12)
$6p_{3/2}$	40.90	4.96	-15.48	0.12	0.00	0.15	30.64	-0.18	30.46	30.460(38)	30.0(7)
$5d_{3/2}$	210.41	16.76	966.23	6.10	40.20	1.38	1241.08	-262.92	978.16	909(15)	966(34)
$5d_{5/2}$	264.18	19.92	1413.30	10.10	61.60	1.76	1770.86	-404.50	1366.36	1353(5)	1351(52)
$7s_{1/2}$	58.74	-0.81	-10.46	-0.03	0.04	0.76	48.23	0.42	48.66	49(4)	48.4(2)
$7p_{1/2}$	171.05	15.42	-14.67	0.88	-0.04	-1.18	171.46	-5.56	165.90	155(4)	152(18)
$7p_{3/2}$	146.23	16.90	-20.64	0.72	0.23	-1.31	142.13	-4.23	137.90	133(2)	128(10)

[†]Experimental results tabulated in Ref. [38], except for $5d_{5/2}$ which is from Ref. [39]; [‡]Theory (CCSDpT) calculations from Ref. [38].

Table 13: Scalar dipole polarisability α_0 for the lowest few states of Cs, calculated using mixed-states (Dalgarno-Lewis) method. Structure radiation and normalisation of states contributions calculated using the sum-over-states approach, considering only the dominating few terms.

State	HF	δRPA	$\delta\Sigma^{(\infty)}$	δQED	δBreit	$\delta\text{SR+N}$	<i>ab initio</i>	$\delta\lambda\Sigma$	Final	Expt. [†]
$6s_{1/2}$	663.58	-73.39	-189.93	1.33	-0.04	-0.96	400.60	-0.49	400.11	400.9(7)
$6p_{1/2}$	1379.7	-60.6	39.83	-0.2	10.9		1369.61	-43.5	1326.1	
$6p_{3/2}$	1620.0	-69.2	138.06	0.7	11.4		1701.03	-66.4	1634.7	

[†]Experimental results tabulated in Ref. [40].

A Appendix

Some useful equations and definitions are given here; see also Refs. [2, 3, 5, 12, 41–43]. Note that notation differs between all these sources, I have introduced some notation not found in the above.

A.1 Many-body wavefunction (Slater determinant)

For a system of non-interaction particles, the many-body wavefunction may be written as a product state (independent particle picture). If each single-particle wavefunction ψ obeys $\hat{h}\psi = \varepsilon\psi$, it clear, e.g., that a two-body product wavefunction $\psi_a(r_1)\psi_b(r_2)$ satisfies the total Hamiltonian:

$$[h(r_1) + h(r_2)]\psi_a(r_1)\psi_b(r_2) = [\varepsilon_a + \varepsilon_b]\psi_a(r_1)\psi_b(r_2). \quad (\text{A.1})$$

This remains true for states where each particle interacts with a common field (e.g., $h = h_0 + V(r)$), as is the basis for mean-field approximations such as Hartree-Fock. For Fermions, the many-body wavefunction must be anti-symmetric under the exchange of any two particles, and must not allow any two particles to occupy the same state. A two-particle state which satisfies this may be written

$$\Psi_{ab}(r_1, r_2) = \frac{1}{\sqrt{2}} [\psi_a(r_1)\psi_b(r_2) - \psi_b(r_1)\psi_a(r_2)]. \quad (\text{A.2})$$

More generally, an N -body wavefunction may be written in the form of a determinant, known as a Slater determinant,

$$\Psi_{ab\dots n}(r_1, r_2, \dots, r_N) = \frac{1}{\sqrt{N!}} \begin{vmatrix} \psi_a(r_1) & \psi_a(r_2) & \dots & \psi_a(r_N) \\ \psi_b(r_1) & \psi_b(r_2) & \dots & \psi_b(r_N) \\ \vdots & \vdots & \ddots & \vdots \\ \psi_n(r_1) & \psi_n(r_2) & \dots & \psi_n(r_N) \end{vmatrix} \quad (\text{A.3})$$

which is an eigenstate of the Hamiltonian

$$H = \sum_i^N h(r_i).$$

Note that the determinant form encodes the Fermion antisymmetry and exclusion principal.

The introduction of explicit interactions between particles [e.g., introducing $V(r_1, r_2)$ into (A.1)] means the wavefunction cannot be written exactly as a single Slater determinant. However, if the interaction terms can be made to be small (e.g., by good choice of mean field), they may be treated perturbatively. The many-body wavefunction can be written as an expansion over Slater-determinant states (many-body perturbation theory); see, e.g., [2, 3]. We will typically refer to the single-particle wavefunctions, ψ , that make up the total N -body Slater determinant, Ψ , as *orbitals*.

A.2 Matrix elements for many-body states

Let F and G be one- and two-particle operators

$$\hat{F} = \sum_i \hat{f}(\mathbf{r}_i) \quad , \quad \hat{G} = \sum_{i<j} \hat{g}(\mathbf{r}_i, \mathbf{r}_j), \quad (\text{A.4})$$

where $f(\mathbf{r}_i)$ acts on the i th electron; $g(\mathbf{r}_i, \mathbf{r}_j)$ acts on the pair of electrons $\{i, j\}$. Here, I use the short-hand notation from Ref. [2]:

$$|\Phi_i^n\rangle = a_n^\dagger a_i |\Phi\rangle,$$

with i, j denoting occupied states (core and valence), and m, n , denoting unoccupied virtual excited states. $|\Phi\rangle$ is a many-body Slater determinant wavefunction including the Hartree-Fock core and the occupied valence states (e.g., we may have $|\Phi\rangle = a_v^\dagger |0_{\text{HF}}\rangle$), see Ref. [2]. Then, we have for diagonal matrix elements:

$$\begin{aligned} \langle \Phi | F | \Phi \rangle &= \sum_i \langle i | f | i \rangle = \sum_i f_{ii} \\ \langle \Phi | G | \Phi \rangle &= \sum_{i<j} (\langle ij | g | ij \rangle - \langle ji | g | ij \rangle) = \sum_{i<j} (g_{ijij} - g_{jiij}), \end{aligned} \quad (\text{A.5})$$

for matrix elements between states that differ by a single orbital:

$$\begin{aligned} \langle \Phi_i^n | F | \Phi \rangle &= \langle n | f | i \rangle = f_{ni} \\ \langle \Phi_i^n | G | \Phi \rangle &= \sum_j (\langle nj | g | ij \rangle - \langle jn | g | ij \rangle) = \sum_j (g_{njij} - g_{jnij}), \end{aligned} \quad (\text{A.6})$$

and for matrix elements between states that differ by two orbitals:

$$\begin{aligned} \langle \Phi_{ij}^{nm} | F | \Phi \rangle &= 0 \\ \langle \Phi_{ij}^{nm} | G | \Phi \rangle &= \langle nm | g | ij \rangle - \langle mn | g | ij \rangle = g_{nmij} - g_{mnij}. \end{aligned} \quad (\text{A.7})$$

A.3 Wigner-Eckhardt theorem

For irreducible (spherical) tensor operator T_q^k (q component of tensor operator of rank k), the Wigner-Eckhardt theorem allows us to define a *reduced matrix element* via:

$$\begin{aligned} \langle n_a \kappa_a m_a | T_q^k | n_b \kappa_b m_b \rangle \\ = (-1)^{j_a - m_a} \begin{pmatrix} j_a & k & j_b \\ -m_a & q & m_b \end{pmatrix} \langle n_a \kappa_a || T^k || n_b \kappa_b \rangle, \end{aligned} \quad (\text{A.8})$$

where the reduced matrix element $\langle || T^k || \rangle$ does not depend on magnetic quantum numbers, and $(::)$ is a $3j$ -symbol [43]. The reduced matrix elements have symmetry relation:

$$\langle j || T^k || j' \rangle = (-1)^{j-j'} \langle j' || T^k || j \rangle^*, \quad (\text{A.9})$$

and obey summation relation:

$$\sum_{m_a, m_b, q} |\langle n_a \kappa_a m_a | T_q^k | n_b \kappa_b m_b \rangle|^2 = |\langle n_a \kappa_a || T^k || n_b \kappa_b \rangle|^2. \quad (\text{A.10})$$

A.4 Coulomb Integrals³⁰

The Coulomb integral g_{abcd} can be expressed:

$$\begin{aligned} g_{abcd} &\equiv \iint d\mathbf{r}_1 d\mathbf{r}_2 \psi_a^\dagger(\mathbf{r}_1) \psi_b^\dagger(\mathbf{r}_2) \frac{1}{|\mathbf{r}_{12}|} \psi_c(\mathbf{r}_1) \psi_d(\mathbf{r}_2) \\ &= \sum_{kq} (-1)^q \langle \kappa_a m_a | C_{-q}^k | \kappa_c m_c \rangle \langle \kappa_b m_b | C_q^k | \kappa_d m_d \rangle R_{abcd}^k, \end{aligned} \quad (\text{A.11})$$

where $\mathbf{r}_{12} = |\mathbf{r}_1 - \mathbf{r}_2|$ is expanded over multiplicities, k :

$$\frac{1}{r_{12}} = \sum_{kq} \frac{r_{<}^k}{r_{>}^{k+1}} (-1)^q C_{-q}^k(\mathbf{n}_1) C_q^k(\mathbf{n}_2), \quad (\text{A.12})$$

with $r_{<} \equiv \min(r, r')$, and C_q^k is a spherical tensor:

$$C_q^k \equiv \sqrt{\frac{4\pi}{2k+1}} Y_{kq}(\mathbf{n}). \quad (\text{A.13})$$

The R_{abcd}^k factor (radial Coulomb integral) is:

$$R_{abcd}^k = \int d\mathbf{r}_1 [f_a(r_1) f_c(r_1) + g_a(r_1) g_c(r_1)] y_{bd}^k(r_1), \quad (\text{A.14})$$

with the symmetric $y_{bd}^k = y_{db}^k$ ‘‘Hartree screening function’’ defined:

$$y_{bd}^k(r) = \int_0^\infty \frac{r_{<}^k}{r_{>}^{k+1}} [f_a(r') f_b(r') + g_a(r') g_b(r')] dr' \quad (\text{A.15})$$

(note some other places call $y_{bd}^k(r)/r$ the Hartree screening function).

It is easy to see that g is symmetric under $r_1 \leftrightarrow r_2$, and on interchange of initial/final states: $g_{abcd} = g_{badc} = g_{cdab} = g_{dcba}$. The R_{abcd}^k factor and has more symmetries: $c \leftrightarrow a$, $b \leftrightarrow d$, $(ac) \leftrightarrow (bd)$:

$$\begin{aligned} R_{abcd}^k &= R_{cbad}^k = R_{adcb}^k = R_{cdab}^k \\ &= R_{badc}^k = R_{bdc a}^k = R_{dabc}^k = R_{dcba}^k. \end{aligned} \quad (\text{A.16})$$

³⁰Functions to calculate Coulomb integrals defined in: `/src/Coulomb/`, and functions for angular coefficients are in: `/src/Angular/`

We also define the anti-symmetrised Coulomb integral [see (A.7)]:

$$\tilde{g}_{abcd} = g_{abcd} - g_{abdc}. \quad (\text{A.17})$$

By making use of the Wigner-Eckart theorem, we can define “angular reduced” equations, which do not depend on magnetic quantum numbers. We define the reduced angular integral:

$$C_{ab}^k \equiv \langle \kappa_a || C^k || \kappa_b \rangle \equiv (-1)^{j_a+1/2} \tilde{C}_{ab}^k, \quad (\text{A.18})$$

$$= (-1)^{j_a+1/2} \sqrt{[j_a][j_b]} \begin{pmatrix} j_a & j_b & k \\ -1/2 & 1/2 & 0 \end{pmatrix} \pi(l_a + l_b + k), \quad (\text{A.19})$$

where \tilde{C}_{ab}^k is a short-hand notation that is useful since $\tilde{C}_{ab}^k = \tilde{C}_{ba}^k$, and $\pi(x) = 1$ if x is even, but $= 0$ if x is odd. C_{ab}^k is non-zero only if

$$|j_a - j_b| \leq k \leq j_a + j_b, \text{ and } l_a + l_b + k \text{ is even.} \quad (\text{A.20})$$

The Coulomb integrals have angular decomposition:

$$g_{abcd} \equiv \sum_k C_{abcd}^k Q_{abcd}^k, \quad (\text{A.21})$$

$$\tilde{g}_{abcd} \equiv g_{abcd} - g_{abdc} = \sum_k C_{abcd}^k W_{abcd}^k, \quad (\text{A.22})$$

where C_{abcd}^k depends on magnetic quantum numbers, and Q is independent of magnetic quantum numbers. Using the graphical formalism [2] (with Lindgren phase choice),

$$C_{abcd}^k = (-1)^{j_a+j_b+1} \begin{array}{c} \begin{array}{ccc} a & & b \\ \uparrow & & \uparrow \\ | & \xrightarrow{k} & | \\ c & & d \end{array} \end{array}. \quad (\text{A.23})$$

The reduced Coulomb integrals Q^k , W^k , and P^k are thus defined:

$$\begin{aligned} Q_{abcd}^k &\equiv (-1)^{k+j_a+j_b+1} C_{ac}^k C_{bd}^k R_{abcd}^k \\ &= (-1)^k \tilde{C}_{ac}^k \tilde{C}_{bd}^k R_{abcd}^k \end{aligned} \quad (\text{A.24})$$

$$\begin{aligned} W_{abcd}^k &\equiv Q_{abcd}^k + [k] \sum_{\lambda} \left\{ \begin{array}{ccc} j_a & j_c & k \\ j_b & j_d & \lambda \end{array} \right\} Q_{abdc}^{\lambda} \\ &\equiv Q_{abcd}^k + P_{abcd}^k \end{aligned} \quad (\text{A.25})$$

(note the exchange of the final two indices *inside* the P^k definition). Q_{abcd}^k is convenient due to symmetries: $c \leftrightarrow a$, $b \leftrightarrow d$, $(ac) \leftrightarrow (bd)$ (same as R). P_{abcd}^k (and thus W_{abcd}^k) is symmetric under the subset:

$$P_{abcd}^k = P_{dcba}^k = P_{cdab}^k = P_{badc}^k. \quad (\text{A.26})$$

Differing notation

Our Q_{abcd}^k differs from $Q_k(acbd)$ defined in Ref. [12] by a factor $(-1)^{k+1}$ (note that the second and third indices are swapped). Our Q^k and W^k are related to the X_k and Z_k of Ref. [2, 3] via a factor $(-1)^{j_a+j_b+1}$:

$$\begin{aligned} X_k(abcd) &\equiv (-1)^k C_{ac}^k C_{bd}^k R_{abcd}^k \\ &= (-1)^{j_a+j_b+1} Q_{abcd}^k \end{aligned} \quad (\text{A.27})$$

$$Z_k(abcd) = (-1)^{j_a+j_b+1} W_{abcd}^k \quad (\text{A.28})$$

Our definition is chosen to make full advantage of the symmetry properties.

A.5 Angular integrals + identities

Clebsch-Gordon coefficients notation

$$\langle j_1 m_1, j_2 m_2 | JM \rangle \equiv (-1)^{j_1-j_2+M} \sqrt{[J]} \begin{pmatrix} j_1 & j_2 & J \\ m_1 & m_2 & -M \end{pmatrix} \quad (\text{A.29})$$

$$\equiv C(j_1, j_2, J; m_1, m_2, M) \quad (\text{A.30})$$

$$\equiv C_{j_1 m_1, j_2 m_2}^{JM}. \quad (\text{A.31})$$

$$|j_1 j_2; JM\rangle = \sum_{m_1, m_2} \langle j_1 m_1, j_2 m_2 | JM \rangle |j_1 m_1\rangle |j_2 m_2\rangle \quad (\text{A.32})$$

Useful identities

$$\sum_{m_b} g_{abab} = [j_b] R_{abab}^0. \quad (\text{A.33})$$

$$\sum_{m_i, j, k, l} g_{ijkl} g_{lkji} = \sum_{\mu} \frac{1}{[\mu]} (C_{ik}^{\mu} C_{jl}^{\mu} R_{ijkl}^{\mu})^2 \quad (\text{A.34})$$

$$= \sum_{\mu} \frac{1}{[\mu]} (Q_{ijkl}^{\mu})^2 \quad (\text{A.35})$$

$$\begin{aligned} \sum_{m_i, j, k, l} g_{ijkl} g_{lkji} &= \sum_{\mu\lambda} (-1)^{\mu+\lambda+1} C_{ik}^{\mu} C_{jl}^{\mu} C_{il}^{\lambda} C_{jk}^{\lambda} \\ &\quad \times \left\{ \begin{array}{ccc} j_i & j_k & \mu \\ j_j & j_l & \lambda \end{array} \right\} R_{ijkl}^{\mu} R_{ijlk}^{\lambda} \end{aligned} \quad (\text{A.36})$$

$$= - \sum_{\mu} \frac{1}{[\mu]} Q_{ijkl}^{\mu} P_{ijkl}^{\mu} \quad (\text{A.37})$$

Some angular integrals + matrix elements

$$\sum_{jm} (2j+1) \begin{pmatrix} j_1 & j_2 & j \\ m_1 & m_2 & m \end{pmatrix} \begin{pmatrix} j_1 & j_2 & j \\ m_1' & m_2' & m \end{pmatrix} = \delta_{m_1 m_1'} \delta_{m_2 m_2'}$$

$$\sum_{m_1 m_2} (2j+1) \begin{pmatrix} j_1 & j_2 & j \\ m_1 & m_2 & m \end{pmatrix} \begin{pmatrix} j_1 & j_2 & j' \\ m_1 & m_2 & m' \end{pmatrix} = \delta_{jj'} \delta_{mm'} \quad (\text{A.38})$$

$$\begin{aligned} \int Y_{l'm'} Y_{lm} Y_{LM} d\Omega \\ = \sqrt{\frac{[l'] [l] [L]}{4\pi}} \begin{pmatrix} l' & l & L \\ 0 & 0 & 0 \end{pmatrix} \begin{pmatrix} l' & l & L \\ m' & m & M \end{pmatrix} \end{aligned} \quad (\text{A.39})$$

$$\sum_{m_l=-l}^l |Y_{lm_l}|^2 = \frac{2l+1}{4\pi}, \quad \sum_m |\Omega_{\kappa m}|^2 = \frac{2j+1}{4\pi} \quad (\text{A.40})$$

$$\langle l_a || C^k || l_b \rangle = (-1)^{l_a} \sqrt{[l_a][l_b]} \begin{pmatrix} l_a & l_b & k \\ 0 & 0 & 0 \end{pmatrix} \quad (\text{A.41})$$

$$r_q = |r| C_q^1 = |r| \sqrt{\frac{4\pi}{3}} Y_{1q}; \quad r_0 = z.$$

$$\langle n\kappa || r_z || n'\kappa' \rangle = (n\kappa | r | n'\kappa') \langle \kappa || C^1 || \kappa' \rangle. \quad (\text{A.42})$$

$$\begin{aligned} \langle J' I F' || T^k || J I F \rangle \\ = (-1)^{F+J'+I+k} \sqrt{[F'] [F]} \left\{ \begin{array}{ccc} J & I & F \\ F' & k & J' \end{array} \right\} \langle J' || T^k || J \rangle \end{aligned} \quad (\text{A.43})$$

where $([a] \equiv 2a+1)$.

From Ch. 13 of Ref. [43]:

$$\begin{aligned} \langle j l s || l || j' l' s' \rangle &= \delta_{ll'} \delta_{ss'} (-1)^{j'+l+s+1} \sqrt{[j] [j'] [l] (l+1)} \left\{ \begin{array}{ccc} j & 1 & j' \\ l & s & l \end{array} \right\} \\ \langle j l s || s || j' l' s' \rangle &= \delta_{ll'} \delta_{ss'} (-1)^{j+l+s+1} \sqrt{[j] [j'] [s] s(s+1)} \left\{ \begin{array}{ccc} j & 1 & j' \\ s & l & s \end{array} \right\}. \end{aligned} \quad (\text{A.44})$$

A 6- j symbol

$$\left\{ \begin{array}{ccc} 1 & 2 & 3 \\ 4 & 5 & 6 \end{array} \right\} \quad (\text{A.45})$$

is non-zero only if each of the triads obey triangle inequality,

$$\Delta(1, 2, 3), \Delta(3, 4, 5), \Delta(2, 4, 6), \Delta(5, 6, 1). \quad (\text{A.46})$$

A.6 Useful definitions/identities

Dirac matrices

Dirac matrices are defined by the relation:

$$\{\gamma^\mu, \gamma^\nu\} = 2g^{\mu\nu}. \quad (\text{A.47})$$

In the Dirac representation, with $\gamma^5 \equiv i\gamma^0\gamma^1\gamma^2\gamma^3$, they are:

$$\gamma^0 = \begin{pmatrix} 1 & 0 \\ 0 & -1 \end{pmatrix}, \quad \gamma^a = \begin{pmatrix} 0 & \sigma^a \\ -\sigma^a & 0 \end{pmatrix}, \quad \gamma^5 = \begin{pmatrix} 0 & 1 \\ 1 & 0 \end{pmatrix}. \quad (\text{A.48})$$

Pauli spin matrices

$$\sigma_x = \begin{pmatrix} 0 & 1 \\ 1 & 0 \end{pmatrix}, \quad \sigma_y = \begin{pmatrix} 0 & -i \\ i & 0 \end{pmatrix}, \quad \sigma_z = \begin{pmatrix} 1 & 0 \\ 0 & -1 \end{pmatrix} \quad (\text{A.49})$$

$$\sigma_i \sigma_j = i\epsilon_{ijk} \sigma_k + \delta_{ij}, \quad [\sigma_i, \sigma_j] = 2i\epsilon_{ijk} \sigma_k \quad (\text{A.50})$$

$$(\boldsymbol{\sigma} \cdot \mathbf{a})(\boldsymbol{\sigma} \cdot \mathbf{b}) = \mathbf{a} \cdot \mathbf{b} + i\boldsymbol{\sigma} \cdot (\mathbf{a} \times \mathbf{b}) \quad (\text{A.51})$$

$$(\boldsymbol{\sigma} \cdot \mathbf{p})y(r)\Omega_{\kappa m} = i\left(y' + \frac{\kappa + 1}{r}y\right)\Omega_{-\kappa, m} \quad (\text{A.52})$$

$$(\boldsymbol{\sigma} \cdot \mathbf{n})\Omega_{\kappa m} = -\Omega_{-\kappa, m}. \quad (\text{A.53})$$

Dirac orbitals (spherical potential, Dirac basis)

$$\phi_{n\kappa m}(\mathbf{r}) = \frac{1}{r} \begin{pmatrix} f_{n\kappa}(r)\Omega_{\kappa m}(\mathbf{n}) \\ ig_{n\kappa}(r)\Omega_{-\kappa, m}(\mathbf{n}) \end{pmatrix}, \quad (\text{A.54})$$

$$\Omega_{\kappa m}(\mathbf{n}) = \sum_{\sigma=\pm 1/2} \langle l, m - \sigma, 1/2, \sigma | j, m \rangle Y_{l, m - \sigma}(\mathbf{n}) \chi_\sigma \quad (\text{A.55})$$

$$= \begin{pmatrix} (-1)^{j-l-1/2} \sqrt{\frac{\kappa+1/2-m}{2\kappa+1}} Y_{l, m-1/2}(\theta, \phi) \\ \sqrt{\frac{\kappa+1/2+m}{2\kappa+1}} Y_{l, m+1/2}(\theta, \phi) \end{pmatrix}, \quad (\text{A.56})$$

where j and l are the total and orbital angular momentum, with

$$\kappa = (l - j)(2j + 1), \quad l = |\kappa + 1/2| - 1/2, \quad j = |\kappa| - 1/2. \quad (\text{A.57})$$

Note that strictly parity $(-1)^l$, not l , is the good quantum number.

References

- [1] H. A. Bethe and E. E. Salpeter, *Quantum mechanics of one-and two-electron atoms* (Plenum Publishing Corporation, New York, 1977).
- [2] I. Lindgren and J. Morrison, *Atomic many-body theory*, 2nd ed. (Springer-Verlag, New York, 1986).
- [3] W. R. Johnson, *Atomic Structure Theory* (Springer, New York, 2007).
- [4] V. A. Dzuba, O. P. Sushkov, and V. V. Flambaum, *Prepr. INP* **82-89** *INP* **82-89** (1982).
- [5] J. Sapirstein, *Rev. Mod. Phys.* **70**, 55 (1998).
- [6] G. B. Arfken, H. J. Weber, and F. E. Harris, *Mathematical Methods for Physicists* (Elsevier, 2013).
- [7] J. C. Slater, *Phys. Rev.* **81**, 385 (1951).
- [8] H. M. Quiney, I. P. Grant, and S. Wilson, *Phys. Scr.* **36**, 460 (1987).
- [9] W. R. Johnson, S. A. Blundell, and J. Sapirstein, *Phys. Rev. A* **37**, 307 (1988).
- [10] K. Beloy and A. Derevianko, *Comput. Phys. Commun.* **179**, 310 (2008), [arXiv:0710.3142](#).
- [11] E. V. Kahl and J. C. Berengut, *Comput. Phys. Commun.* **238**, 232 (2019), [arXiv:1805.11265](#).
- [12] V. A. Dzuba, V. V. Flambaum, and O. P. Sushkov, *J. Phys. B* **17**, 1953 (1984).
- [13] A. Dalgarno and J. T. Lewis, *Proceedings of the Royal Society A* **233**, 70 (1955).
- [14] J. S. M. Ginges and V. V. Flambaum, *Phys. Rep.* **397**, 63 (2004).
- [15] V. A. Dzuba, J. C. Berengut, J. S. M. Ginges, and V. V. Flambaum, *Phys. Rev. A* **98**, 043411 (2018), [arXiv:1805.04989](#).
- [16] N. L. Manakov, V. D. Ovsiannikov, and L. P. Rapoport, *Phys. Rep.* **141**, 320 (1986).
- [17] W. R. Johnson, C. D. Lin, K. T. Cheng, and C. M. Lee, *Phys. Scr.* **21**, 409 (1980).
- [18] W. R. Johnson, *Adv. At. Mol. Opt. Phys.* **25**, 375 (1989).
- [19] J. J. Sakurai, *Modern Quantum Mechanics* (2011).
- [20] V. A. Dzuba, V. V. Flambaum, P. G. Silvestrov, and O. P. Sushkov, *J. Phys. B* **20**, 1399 (1987).
- [21] A. Kramida, Y. Ralchenko, J. Reader, and The NIST ASD Team (2018), *NIST At. Spectra Database (ver. 5.6.1)* [Online], <http://physics.nist.gov/asd>.
- [22] V. A. Dzuba, V. V. Flambaum, P. G. Silvestrov, and O. P. Sushkov, *Phys. Lett. A* **103**, 265 (1984).
- [23] V. A. Dzuba, V. V. Flambaum, P. G. Silvestrov, and O. P. Sushkov, *J. Phys. B* **18**, 597 (1985).
- [24] V. A. Dzuba, V. V. Flambaum, P. G. Silvestrov, and O. P. Sushkov, *Phys. Lett. A* **131**, 461 (1988).
- [25] A. A. Abrikosov, L. P. Gorkov, and I. E. Dzyaloshinski, *Methods of Quantum Field Theory in Statistical Physics* (Pergamon Press, 1965).
- [26] V. A. Dzuba, V. V. Flambaum, and O. P. Sushkov, *Phys. Lett. A* **140**, 493 (1989).
- [27] V. A. Dzuba, V. V. Flambaum, and J. S. M. Ginges, *Phys. Rev. D* **66**, 076013 (2002).
- [28] V. A. Dzuba, *Phys. Rev. A* **78**, 042502 (2008).
- [29] S. A. Blundell, D. S. Guo, W. R. Johnson, and J. Sapirstein, *At. Data Nucl. Data Tables* **37**, 103 (1987).
- [30] W. R. Johnson, Z. W. Liu, and J. Sapirstein, *At. Data Nucl. Data Tables* **64**, 279 (1996).
- [31] W. R. Johnson, S. A. Blundell, and J. Sapirstein, *Phys. Rev. A* **37**, 2764 (1988).
- [32] J. B. Mann and W. R. Johnson, *Phys. Rev. A* **4**, 41 (1971).
- [33] A. Derevianko, *Phys. Rev. A* **65**, 012106 (2001).
- [34] V. V. Flambaum and J. S. M. Ginges, *Phys. Rev. A* **72**, 052115 (2005).
- [35] J. S. M. Ginges and J. C. Berengut, *J. Phys. B* **49**, 095001 (2016).
- [36] J. S. M. Ginges and J. C. Berengut, *Phys. Rev. A* **93**, 052509 (2016), [arXiv:1603.09116](#).
- [37] G. Toh, A. Damitz, C. E. Tanner, W. R. Johnson, and D. S. Elliott, *Phys. Rev. Lett.* **123**, 073002 (2019), [arXiv:1905.02768](#).
- [38] M. S. Safronova, U. I. Safronova, and C. W. Clark, *Phys. Rev. A* **94**, 012505 (2016), [arXiv:1605.05210](#).
- [39] S. Pucher, P. Schneeweiss, A. Rauschenbeutel, and A. Darea, *Phys. Rev. A* **101**, 042510 (2020), [arXiv:1912.10089](#).
- [40] P. Schwerdtfeger and J. K. Nagle, *Mol. Phys.* **117**, 1200 (2019).
- [41] L. D. Landau and E. M. Lifshitz, *Quantum Mechanics: Non-relativistic Theory* (Pergamon, Oxford, 1977).
- [42] I. I. Sobelman, *Atomic Spectra and Radiative Transitions* (Springer, Berlin, Heidelberg, 1992).
- [43] D. A. Varshalovich, A. N. Moskalev, and V. K. Khersonskii, *Quantum Theory of Angular Momentum* (World Scientific, Singapore, 1988).